SYNTHESIS AND CHARACTERIZATION OF PURE AND Bi_2O_3 DOPED BARIUM HEXA - FERRITES

A Tnesis Submitted
In Partial Fulfilment of the Requirements
for the Degree of

MASTER OF TECHNOLOGY

by

H. KRISHNAN

to the

MATERIALS SCIENCE PROGRAMME

INDIAN INSTITUTE OF TECHNOLOGY, KANPUR

MAY, 1987

MSP-1987-M-KRI-SYN

TO MY BELOVED GRAND FATHER
LATE SHRI A. KRISHNA IYER

CONTENTS

LIST OF TABLES

--

LIST OF FIGURES

--

ABSTRACT

In the present study, pure and Bi_2O_3 doped Barium hexaferrite has been synthesized using ceramic method. The samples are prepared by sintering method. During this process, doped Bi_2O_3 promotes the liquid phase sintering and thereby reducing the sintering temperature. The samples has been characterized using techniques of x-ray diffraction, magnetization, mechanical deformation, electrical and dielectrical behaviour. The effect of sintering temperature and time on these properties have been discussed in detail.

The first chapter of the thesis deals about crystal structu magnetic structure, general method of synthesis and applications of ferrites.

In the second chapter the subject matter related to magnetic properties, electrical and dielectrical properties of ferrite are described.

The third chapter describes the synthesis method, character ization and results of experimental observations.

Conclusions have been discussed in 4th Chapter.

--

CHAPTER - 1

THEORY OF HEXAGONAL FERRITES

ABSTRACT

In the present chapter an attempt is made to describe the classification of hard ferrites and their chemical, crystallographic and magnetic structures. Their method of preparation and uses are also presented.

1.1 Introduction :

The magnetic oxides possessing hexagonal structures are known as Hexaferrites. Most important of these is the well known material barium hexaferrite ($BaO.6Fe_2O_3$). This was first developed by Philips Research Laboratory and was called Ferroxdure [1]. The other important hexaferrite is strontium ferrite ($SrO.6Fe_2O_3$). These ferrites remain permanently magnetized even after the removal of magnetic field due to its large magneto-crystalline anisotropy. These materials are therefore used as permanent magnets and they are also known as hard magnetic materials. A broad classification based on chemical constitution for ferrites under this class is given below [2].

$MO.6Fe_2O_3$ M type

$BaO.2MO.8Fe_2O_3$ - W type

$2(BaO.MO.3Fe_2O_3)$ - Y type

$3\ BaO.2MO.12Fe_2O_3$ - Z type

Where M is a divalent metal ion. Out of these, barium hexaferrite is discussed in detail.

1.2 Crystal Structure :

The barium ferrite $BaO.6Fe_2O_3$ and strontium ferrite $SrO.6Fe_2O_3$ materials are commercially important materials. They possesses the identical crystal structure as magneto-plumbite $PbO.6[(Fe_{1.25}Mn_{0.6}Al_{0.8}Ti_{0.08})_2O_3]$ [3]. In the case of pure Barium hexaferrite, Fe ions occupy the same positions as the mixtures of Fe, Mn, Al and Ti in the mineral magnetoplumbite. The Ba^{2+} and O^{2-} ions are both large and about the same size ($r_{Ba^{2+}} = 1.43A^{\circ}$, $r_{O^{2-}} = 1.32\ A^{\circ}$) [4]. They are stacked in a close packed fashion. The smaller Fe^{3+} ions are located in the interstice The barium hexaferrite unit cell is as shown in the figure (1.1), consists of 10 close packed layers having mixed hexagonal (h) and cubic (k) stacking. The stacking sequence this can be written as hhhkkhhhkk in Zhadnov symbol and as (111 2 111 2) in the Jagodzinsk [5]. Thus it essentially consists of 4 blocks, two hexagonal (hhh) and two cubic (kk). The eight close packed layers consist of purely O_2 ion, and remaining two (i.e., second and seventh hexagonal layer from the bottom of the cell) consists of three oxygen and one Barium ion. Each layer consists of 4 large ions. Thus the oxygen and barium ion close packed lattice consists of three types of interstitials namely, tetrahedral (surrounded by four O_2 ions), hexagonal (surrounded by five oxygen ions, three on the bottom and two on the top) and octahedral (surrounded by eight oxygen ions). The unit cell as a whole has hexagonal symmetry with $a = b = 5.88A^{\circ}$ and $C = 23.2A^{\circ}$, and it contains two barium hexaferrite molecules. The filling of interstitials in hexaferrite by Fe^{3+} ion is identical to those of spinels.

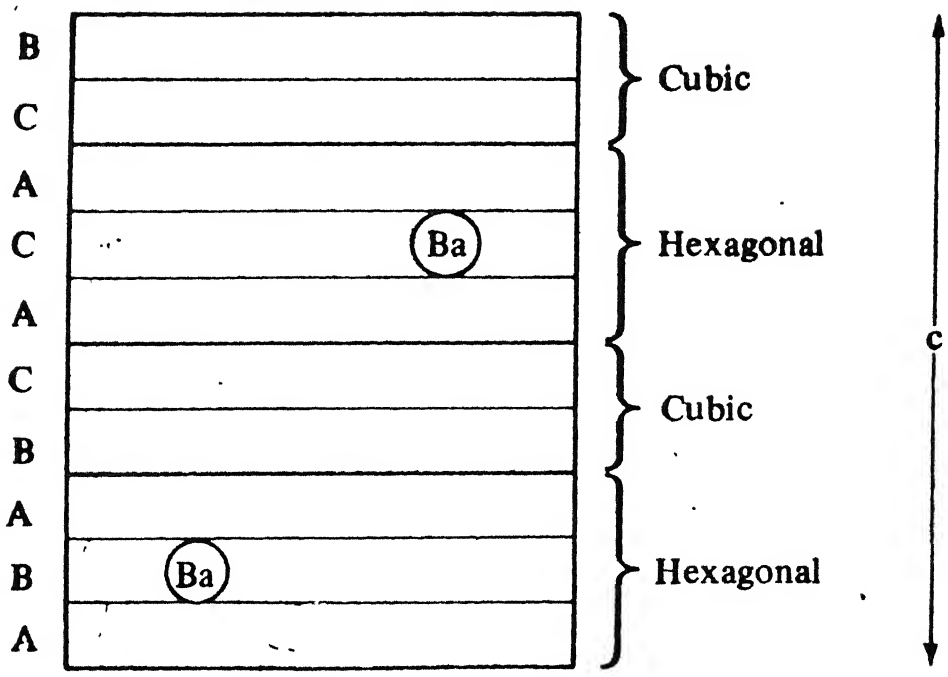

Fig. 1.1 Schematic representation of the barium ferrite structure.

1.3 Magnetic Structure :

In the case of barium ferrite, the only magnetic ions present is Fe^{3+} with a moment of 5 Bohr magneton (μ_B) and they are 24 in an unit cell. These are located in three crystallographically different kinds of sites (i.e.) 4 at tetrahedral site, 18 at octahedral sites and 2 at hexahedral site. The Fe^{3+} ions have their moments normal to the basal (a-b) plane of the oxygen layers, and thus parellel or anti-parellel to the c-axis (< 000.1>) of the hexagonal cell. The arrangement of 24 Fe^{3+} ions each with spin 5 μ_B is given below with their spin directions [6].

Tetrahedral sites (4 nearest O^{2-} neighbours), 4↑

Octahedral sites (b nearest O^{2-} neighbours), 4↑ 14↓

Hexagonal sites (5 nearest O^{2-} neighbours) 2↓

This gives a net magnetic moment 8 x 5 = 40 μ_B per unit cell. The theoretical saturation magnetization M_s is then calculated as follows:

M_s = Magnetic moment of the unit cell/ volume of the unit cell

$$= \frac{40 \times 0.927 \times 10^{-20}}{694 \times 10^{24}} \text{ erg/Oe cm}^3$$

$$= 538 \text{ emu/cm}^3$$

1.4 Comparision of Hexagonal Ferrites with Spinel Ferrites:

Spinel materials are soft materials having high initial permiability, high saturation magnetization, low coercivity and low (BH) product. Hexagonal ferrites on the

otherhand possess high coercivity, high (BH) product, low saturation magnetization and low initial permiability [6]. The arrangement of cations are entirely different in these two ferrites In spinel case there are 2 sites for cations, namely the tetrahedral sites and octahedral sites. But in hexagonal ferrites there are 3 sites, namely tetrahedral, octahedral and hexahedral. Curie temperature of hexa ferrites are low compared to spinel ferrites. However Curie temperature of hexaferrites are likely to get affected lesser by the metal ion substitution for Fe^{3+} ion. Hexaferrites are also grain oriented or anisotropic materials. Their commerical utility is based upon the strength coupling of magnetization to the axial direction. This characteristic strong coupling produces high anisotropic materials of the order of 10^6 erg/cm^3 in contrast to 10^4 to 10^5 erg/cm^3 of spinels. Due to this high anisotropy, hexaferrites are used as permanent magnets.

1.5 Comparision of Hexagonal Ferrites with Metallic Magnets :

In general hard magnetic materials are classified into two groups, one is metallic (alloys) and the other is ferrite magnet materials. Magnetic metals are more dense and they are capable of greater magnetic moments and Curie temperature (BH) product is al higher for magnetic metals as compared to ferrites. But they are of limited use because of their high electrical conductivity and high manufacturing cost. Alloying can decrease conductivity but it will affect mechanical and magnetic properties of the material. Hexagonal ferrites are hard ferrites and they are very stable and difficult to demagnetize either by external fields or by

mechanical shock they usually possess a negative temperature coefficient of remanence which may be of the order of 0.2% per deg. °C [7]. This volume is ten times greater than that of a metal alloy magnet and although this is often a disadvantage, it can occasionally be put to practical use. Ferrite magnets are resistant to demagnetization by heating, provided the Curie temperature is not approached too closely. Saturation magnetization of ferrite materials are low compared to metal magnets. Ferrite magnets are more economical due to its easy manufacturing processes. Raw materials of these ferrites are very cheap and very simple to synthesis.

1.6 Preparation :

Polycrystalline ferrites are usually formed by a kind of solid state reaction. A sintered polycrystalline body is not truely a solid but contains many pores. The quantity size, shape and distribution of both crystal grains and pores through the body, will vary with different synthesizing techniques, firing temperatures, atmosphere and times. As a result, numerous processes have been developed till date. They are presented below:

1.6.1 Oxide method :

High purity oxide materials are mixed in the stoichiometric proportions and made to react at high temperature (1200°C to 1300°C). The extent and rate of solid state reaction depend upon factors such as particle size, temperature, time, chemical nature and crystal structure and the reactants. mixing of starting

powders are often performed by wet milling for a long period in a rubber lined pot using stainless steel balls. Dry mixing of materials is unsuitable because sufficient dispersion will not be obtained. After milling, mixture is dried and pressed into pellets before presintering. Organic polymer such as polyvinyl alcohol is used as a binder. To obtain a higher degree of homogeneity, it is often necessary to crush the presintered pellets and then give final sintering at higher temperature after pelletization(desire shapes). During pelletization for final sintering, magnetic field is applied to orient the grains of the material in a particular direction. This magnetic treatment makes the material anisotropicand increases the $(BH)_{max}$. Isotropic ferrites do not undergo this magnetic treatment. Usually, low sintering temperature are preferred because high temperature sintering accentuates volatility and induces violent changes [8]. It also results in inhomogeneous surface layers that degrade the magnetic performance. High temperature sintering results in grain growth and consequent reduction in coercivity.

1.6.2 Decomposition method:

In this method, instead of using oxides as starting materials, one may use salts such as carbonates, nitrates and oxalates. These salts are mixed in the required proportions, then sintering in air is done. This produces the oxides by thermal decomposions. In other words, process is similar to the oxide method and yet relizes upon a mechanical process to produce the uniform dispersion of the constituents.

1.6.3 Coprecipitation Method [10]:

To avoid the lengthy milling processes involved in wet mixing, attempts have been made to simultaneously precipitate the required hydroxides from a solution, so that precipitate containing the required metals in correct proportions, which is obtained. are already intimately mixed, Knowledge of the solubility product of the substance is essential in order to determine the pH value for complete precipitation. The mixed cations are precipitated out by a strong base (usually NaOH) in a soluble pH and dilution range. The pH is also related to solubility product. The most important feature of this method is the intimate mixing of ions on the atomic level, so that subsequent nucleation and crystallization can occur at low temperatures. This behaviour prevents grain growth and the particles are perfect in that they are free from stresses and strains caused by particle diminution in milling. High coercivity thus can be expected from this method.

1.6.4 Electrolytic Co-precipitation [11]:

In this method, the composition is formed by electrolysis from the anode, which is made of metal. Type of metal would be dependent on the oxide required.

1.6.5 Hot Pressing [12]:

High quality permanent magnet materials are also prepared by pressing very fine ferrite powders at high temperatures. For this process, pressure, temperature are to be optimized to reduce particle size, so that coercivity of the

materials will be increased.

1.6.6 Other Methods:

Single crystals of pure and doped $M.Fe_2O_3$ (M-Ba, Sr) have been grown from different solvents by spontaneous nucleation growth [13]. Strong improvement in crystal size was obtained using Na_2O-Fe_2O_3 flux. Thin film deposition methods are also employed for Ba ferrite [14].

1.7 Applications of Hard Ferrites :

Hard ferrite magnets have naturally first been used for purposes where their merits are outstanding and their defects are unimportant. For toys, novelties cheapness is important than great magnetic strength. Low magnetization and high coercivity of these materials makes these materials specially suitable for applications where large demangetizing fields are encountered. Barium ferrite magnets are used in loud speakers circuits, magnets for focussing electron beams, for fixing one object to another. Also barium ferrite magnets are used for oil filters, electric generators and motors etc. Barium ferrites are also used as magnetic chucks to hold work piece during grinding, milling, plaining and turning. These ferrites found only limited use in recording surfaces, primarily because the high coercivity requires that the material of the writing head have a saturation flux density. However, the high coercivity of this material gives the recording surface a unique ability to withstand, high demagnetizing fields (erasing fields). This property has been utilized specially for the two major applications

In the first application, master tapes are made from high coercivity hexaferrites which are used to transfer information to copy tapes by bringing two tapes (master and copy tapes) together in the presence of a magnetic field. The transfer field should be high enough so that the combination of transfer plus signal fields are enough to switch the information in the copy tape, yet it would be advantageous to use very high coercivity master tapes. The second application is in magnetic stripes on credit cards and magnetic badges. Due to there high resistivity and large uniaxial magnetocrystalline energy, these ferrites are used in microwave communication and radar systems as high frequency resonant devices such as tunable filters, gyrators and isolators etc. Ferrite magnets are having very low eddy current losses due to its high resistivity and they are suitable for providing a polarizing field in inductors and transformers. Examples are unidirectional pulse transformers, polarized relays, microphones and telephone circuits.

REFERENCES :

1. J.J. Went, G.W. Ratheman, E.W. Gorter and G.W. Vanoosterhont "Ferroxdure, a class of new Permanent Magnet Materials", Philips Technical Review. Vol 13 (7) 194-208 [1951-52].

2. B.D. Culity, " Introduction to Magnetic Materials", Wesley Publishing Company, 1972.

3. K.J. Standley, "Oxide Magnetic Materials", Monographs on the Physics and Chemistry of Materials, 1962.

4. V.M. Goldschimit "Ionic radii of Various Elements", p. 106 John Wiley and Sons, London, 1975.

5. P. Krishna, 'Characterization of Polytype Structures'' (1976)

6. F. Bradley, " Materials for Magnetic Functions", Hyden Book Company, Inc. New York.

7. M.G. Say 'Magnetic Alloys and Ferrites", Whit Fuairy Press, 1954.

8. M.C.D. and J.C. Jeschkke, "Single domain properties in Hexagonal ferrites", Journal of Applied Physics 34,1271- 1274 (1963).

9. K. Honeda, C. Miyahoma and H. Kojima, " Preparation of high Coercivity $BaO.6Fe_2O_3$", Journal of American Ceramic Society 57188 354-57 (1974).

10. N.K. Ghosh, M. Tech. Thesis Met. Engg. I.I.T. Kanpur, 1981.

11. E.P. Wonlfarth, " Ferromagnetic Materials" Vol. (4) North-Holland Publishing Company.

12. T.M. Oron, 'Ba ferrites-hot pressing process for preparing high quality material from very fine powders", IEEE Trans. Mag. 1452-54 Sept. 75.

13. J.M. Desvigues, H. Le Gall, M. Laberyrie, J. C. Mage, T.M. Cobinsion, "Improvement of Hexaferrites, Crystal Growth Reproducibility and Characterization", Journal De Physique 46 p. 326-331, Sept. 1985.

14. Morisicko, A.M. Matsurroto and Minaoe, 'C-axis Orientation of Hexagonal films prepared by r.f. Sputtering", IEEE Trans. Magentics, 5PG4, 1981-82.

15. E.P. Wohlfarth, "Ferromagnetic Materials," Vol. (3), North Holland Publishing Company (1982).

CHAPTER - 2

PROPERTIES OF HEXAGONAL FERRITES

ABSTRACT

The present chapter deals with electrical, dielectric, magnetic and microwave properties of hexaferrites.

2.1 Magnetic Properties of Barium Hexaferrites:

Several magnetic properties of the barium ferrites are presented in the table 2.1. Measurements of polycrystalline $BaO.6Fe_2O_3$ at liquid hydrogen temperature and in fields upto 26000 Oersteds give theoretical value of specific saturation magnetization 101 emu/gm [1], however at room temperature 20°C it was found to be 72 emu/gm. Various parameters like saturation magnetization, ramanance, hysteresis and coercivity of these materials are studied. The origin of these properties and their variations, depending on method of processing and other physical factors are discussed in the subsequent sections.

2.1.1 Coercivity:

The coercivity is defined as the field applied in reverse direction to demagnetize the magnetized specimen. Now we will see the various factors influencing the coercivity.

(a) Particle size:

Domains are formed in order to reduce the magnetostatic

Table 2.1 : Magnetic properties of barium hexaferrite

S.No.	Property	Value	Reference
1.	Saturation magnetic moment per unit mass (σ_s)	70 gauss cm^3/gm	[1]
2.	Remanent induction (Br)	2050 gauss	[1]
3.	Coercive force (H_c)	2400 Oe	[14]
4.	$(BH)_{max}$	0.85×10^6 .gauss Oersted	[14]
5.	Curie temperature (T_c)	450°C	[8]
6.	Anisotropy constant (K)	3.3×10^6 erg/cm^3	[14]
7.	Temperature Coefficient of remanent induction	-0.2%/C°	[14]
8.	Temperature coefficient of induction in working point	-0.1.5%/C°	[14]
9.	Working point	B 1000 gauss H -850 Oe	[14]

energy, size of the domains is a balance between the reduction of magnetostatic energy by the formation of domains and the increase in energy caused by increased domain wall per unit volume. However, when we decrease the material dimensions below some critical size, we encounter strikingly different behaviour associated with domain structures and magnetization processes unique to fine particles [2] Domain boundary motion ceases to play a significant role because the particle becomes too small to contain domain boundaries. Radical changes in permiability and coercivity are then observed. A spherical particle of diameter 'd' has an associated magnetostatic energy of E_m [2].

$$E_m = \pi^2 d^3 M_s^2/9 \qquad (2.1)$$

This energy can be cut into half by dividing the particle into two domains seperated by a domain boundary and this introduces the domain boundary energy of E_b^1

$$E_b^1 = \frac{\pi d^2 E_b}{4} \qquad (2.2)$$

where E_b' is equilibrium boundary energy. At large domain particle diameters, this boundary energy is negligible compared to magnetostatic energy and hence multidomain structure is energitically favoured. However, with deceasing particle size the magnetostatic energy falls off more rapidly than the boundary energy. Therefore, at some particle diameter the above two energies will exactly balance. This is the critical diameter for single domain particle. It can be shown that critical diameter d_c [2].

$$d_c = 9 \left(\frac{kT_c K}{a} \right)^{1/2} n_s^2 \qquad (2.3)$$

where T_c is the Curie temperature

k is Boltzmann constant

K is crystal anisotropy constant

a is interatomic distance

M_s is saturation magnetization

Domain boundary motion plays an important role in the magnetization of bulk materials. In the absence of domain boundaries (i.e.) for single domain particles, there are three general ways by which the particles can reverse their magnetization under the influence of demagnetization field.

1. By domain reaction
2. By changing the single domain structure (i.e.) nucleating and growing a reverse domain, which requires the introduction of domain boundary energy [1].
3. By fanning and curling [1]

b. Crystal anisotropy :

In the absence of other influences, the magnetization vector of a spherical single domain particle is directed along an easy crystallographic direction to minimize the magneto crystalline anisotropy energy. To rotate the magnetization vector through a more difficult crystal direction requires the application of a reverse field H_c [1]

$$H_c = 2k / M_s \qquad (2.4)$$

where k is magnetocrystalline anisotropy energy constant.

C.. Strain anisotropy:

It has been found that mechanical strain increases the coercive force of a single domain particle by $3\lambda T / M_S$ [2]. where 'λ' is magneto-striction constant, and 'T' is applied stress.

This effect is quite similar to the effect of crystal anisotropy: in order to rotate the magnetization vector the particle must pass through a region of high anisotropy with respect to the stress.

d. Shape Anisotropy:

An elongated single domain particle free from crystal or strain anisotropy will direct its magnetization vector along major axis, where the demagnetizing factor is a minimum and magnetostatic energy is therefore lowest. This effect has been exploited in the case of metalic magnets like 'AlNiCo' and ESD magnets [3].

2.1.2 Saturation magnetization:

Saturation magnetization (M_S) is the maximum value of magnetization (where magnetization is total magnetic moment per unit volume and in Cgs system its unit is gauss) for a ferromagnetic or ferrimagnetic material [4]. We use the term σ_S for specific magnetization which is total magnetic moment per unit mass. Its unit is emu/gm or in cgs system gauss cm^3/gm. Saturation magnetization decreases with increasing milling time of initial raw mixture, due to the formation of soft magnetic phase. It can

be overcome by annealing the sample (5.).

2.1.3 Remnant Magnetization:

Remnant magnetization is defined as the residual magnetization remaining in the sample even after magnetic field is removed. In the case of isotropic ferrites, the preferred directions of mangetization of the constituent particles are oriented at random, in that case remanance is equal to half of the saturation magnetization value [6]. Remnanance can be increased considerably by pressing the powder in a magnetic field before sintering it.

2.1.4 Hysteresis :

In an external magnetic field, the favourably oriented domains grow at the expense of those aligned unfavourably to the field. Finally at larger fields, all domains are oriented parallel to the field due to rotation of magnetization-vectors. Upon the removal of external saturating magnetic field in reverse-direction, the same path will not be traced. This is due to irreversible domain wall movements, cousing the phase lag between external field and magnetization leads to an open loop. This is called hysteresis loop. The case with which the magnetization may be changed by a given magnetic field depends on the anisotropy and structural homogeneity of the material to a large induced magnetization for a given magnetic field [7].

2.1.5 Curie temperature :

It is the temperature at which spontaneous magnetization of

ferrite vanishes. Magnetization will cancel at Curie temperature. Below the Curie temperature sublattice magnetization (hence net megnetization) changes with temperature because the ordering tendency of exchange energy is opposed by disordering effect of thermal energy [8].

2.1.6 Magnetic Losses in Hard Ferrites:

Ferrites can have electrical, magnetic and mechanical losses that must be considered individually for each set of operating conditions [9]. It is essential to attain low losses at the levels of any device. Since increased losses will results in excessive heating, decreased sensitivity and increased attenuation all of which will degrade the system (device) performance. Magnetic losses result due to (a) eddy current loss (b) hysteresis loss (c) losses due to domain wall relaxation and (d) losses due to domain rotation resonance. Residual loss depends on the frequency (f) but not on the field strength. Eddy current loss rises as the square of frequency (f^2) and is independent of field strength. Hysteresis loss is a function of both frequency (f) and field strength B_{max}.

2.2 Electrical and Dielectric Properties of Hexaferrites:

The electrical properties play an important part in many applications. Electrical conductivity promotes eddy currents and prevents high frequency fields penetrating appreciably below the surface (skin effect). The dielectric constant and corresponding

loss angle decides the applicability of ferrites to microwave applications. The underlying theory of ferrites is therefore presented below.

2.2.1 Dielectric Constant and Resistivity of Hexaferrites:

The dielectric properties of a polycrystalline ferrite may vary markedly, depending upon the heat treatment given to it during preparation. The oxygen dissociation pressure [10] over Fe_2O_3 of a $Mo.6Fe_2O_3$ increases rapidly over 1200°C. This may lead to the formation of some divalent iron (FeO). Owing to the presence of Fe^{3+} and Fe^{2+} ions on the same lattice grid leads to high electrical conductivity due to electron hopping mechanism. If the material is cooled in an oxygen atmosphere it may lead to formation of high resistivity thin film around grain boundaries. This occurs due to fast migration of oxygen ion through pores and grain boundary resulting to oxidation of divalent iron . As they have been fired and cooled in different ways, they differ in Fe^{2+} content. Hence they differ in dielectric constant and resistivity due to their inhomogeneous dielectric structure.

Koops [11] assumed that both the grains and boundaries can be represented by parallel R-C circuits. A series combination of these parallel circuits would then represent the behaviour of inhomogeneous dielectric as a whole. This is shown in Fig. [2.1] (a, b and c).

C_p and R_p are the equivalent parallel capacitance and

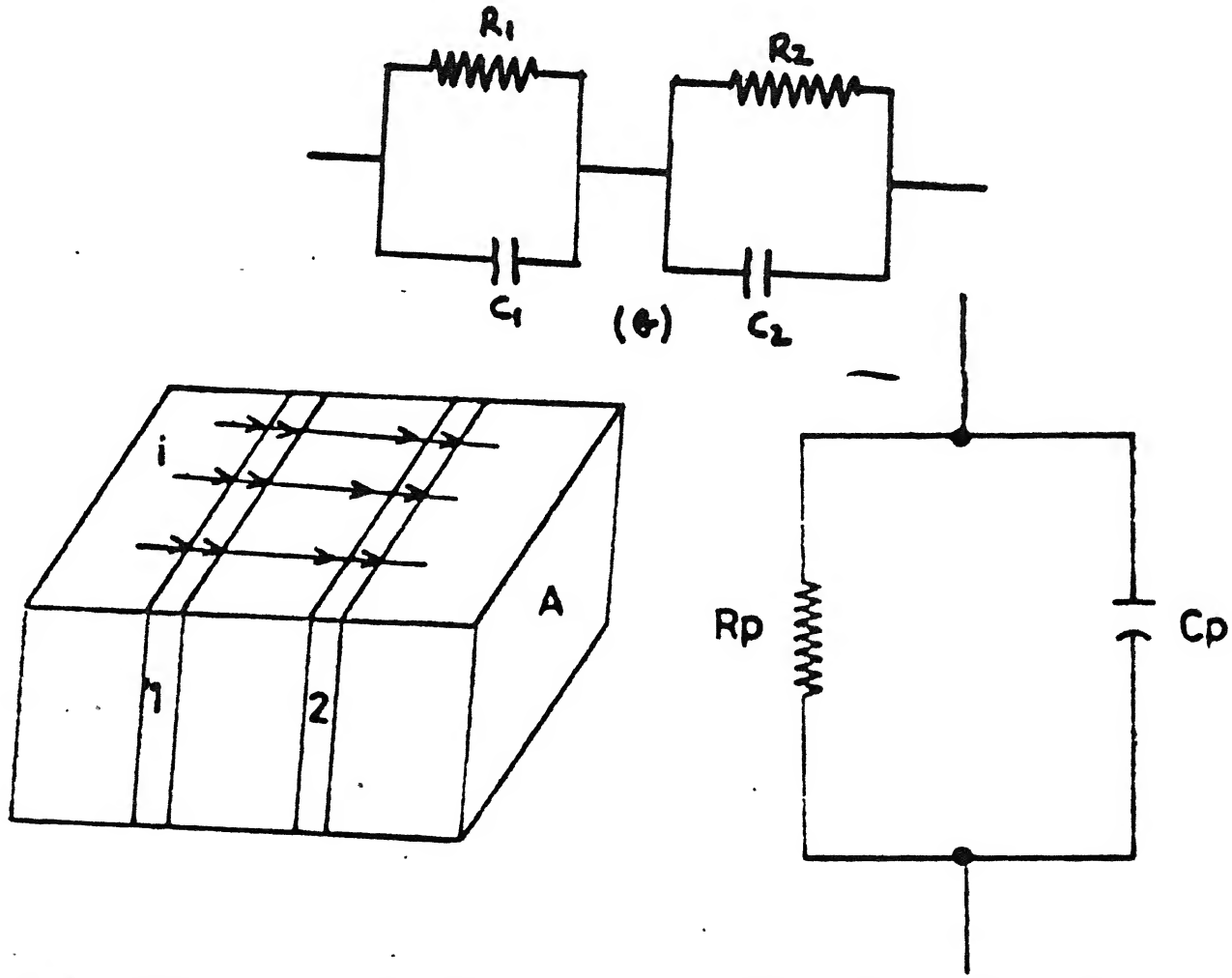

(a) Inhomogenous Dielectric Structure

(c) Equivalant Circuit of Ferrite Dielectric

FIG.2.1 Polycrystalline Structure of Ferrites -Dielectric Structure.

and equivalent parallel resistance respectively in Fig. [2.1 (c)]. The admittance Y_p of the circuit is shown in Fig. [2.1(b)] is

$$Y_p = 1/R_p + j\omega_p \qquad (2.1)$$

where $R_p = \rho_p \, d/A \qquad (2.1\ (a))$

$$C_p = \epsilon_o \epsilon_p \, A/d \qquad (2.1\ (b))$$

and ρ_p and ϵ_p are the resistivity and dielectric constant of the ferrite. A is cross-sectional area of the specimen; l is the length between 2 electrodes.

When A.C. field is applied on dielectric material which does not have free charges, this causes periodic polarization. However polarized change, lag behind applied A.C. field. Under such circumstances losses in the capacitor are represented by a complex dielectric constant

$$\epsilon = \epsilon'_p - j\,\epsilon''_p \qquad (2.2)$$

where ϵ'_p is real part of complex dielectric constant, ϵ''_p is imaginary part of complex dielectric constant under experimental conditions. R_p is quite large and thus admittance is

$$Y_p = j\omega c_p = j\omega \epsilon_o \epsilon \frac{A}{l} \qquad (2.3)$$

$$\therefore\ Y_p = j\omega \epsilon_o \frac{A}{l} \left[\epsilon'_p - j\,\epsilon''_p \right] \qquad (2.4)$$

Equating equations (2.1 with (2.4) we have

$$\frac{1}{R_p} + j\omega c_p = j\omega \epsilon_o \frac{A}{l} \left(\epsilon'_p - j\,\epsilon''_p \right) \qquad (2.5)$$

Comparing real and imaginary parts on both sides

$$\epsilon''_p = \frac{1}{W \epsilon_0 A R_p} = \frac{1}{\omega \epsilon_0 \rho} = \frac{\sigma}{\omega \epsilon_0} \qquad (2.6)$$

It is imaginary component of complex dielectric constant, but it is real, usually called as dielectric loss,

$$\therefore \text{ Dielectric loss } (\epsilon''_p) = \frac{\sigma}{w \epsilon_0} \qquad (2.6(a))$$

and $$\epsilon'_p = C_p \times \frac{1}{A \epsilon_0} \qquad (2.6(b))$$

It is a real component, known as dielectric constant. In the phase diagram, δ is the phase angle between ϵ'_p and ϵ''_p. Tan δC loss tangent, is the measure of dissipation C loss) and it can be expressed as

$$\tan\delta = \epsilon''_p / \epsilon'_p \qquad (2.7)$$

After combining equations (2.2) to (2.6) it leads to

$$\text{Tan}\delta = \frac{1}{wC_p R_p} = \frac{\epsilon''_p}{\epsilon'_p} = \frac{1}{w \epsilon_0 \epsilon_p} \qquad (2.8)$$

Since loss tagent is (tanδ) can be taken as D (Dissipation factor) directly from admittance bridge. Then quality factor of the ferrite can be given by:

$$Q = \frac{1}{\tan\delta} = \frac{1}{D} = wC_p R_p \qquad (2.9)$$

Quality factor tells about how much energy is dissipated in one complete cycle.

Determing the admittance using electric circuit from Fig. (2.1(b)) and equating with equation (2.1) with following assumptions

$x = d_1/d_2 << 1$

$\rho_1 >> \rho_2$

$\rho_1 > \rho_2$

$x\rho_1 > \rho_2$ by a reasonable factor

$\epsilon_1 = \epsilon_2$

where d_1 = grain boundary thickness

d_2 = grain size

$x = \left(\frac{d_1}{d_2} \right)$ is the ratio of thickness of the grain boundary layer to the thickness of crystallites.

Koops arrived at

$$\rho_p = \rho_2 + \frac{x \rho_1}{1 + c' \frac{\rho_1 \rho_2 w^2}{x}} \qquad (2.10)$$

where,

ρ_1 and ρ_2 are resistivity of layers which are marked (a) and (2) in Fig. (b).

$$\epsilon_p = C_2 + \frac{\epsilon_2 / x}{1 + c' \rho_2^2 / \frac{w^2}{x^2}} \qquad (2.11)$$

These 2 above equations tells low resistivity and dielectric constant relax with applied frequency.

If the relevant dimension d c a ferrite sample is larger than half as the wavelength inside the ferrite medium,

standing waves are set up which give rise to high magnetic and dielectric losses. This phenomenon is known as dimensional resonance

$$d \qquad d > \lambda_m / 2 = C / 2f \frac{1}{\sqrt{\mu_r \epsilon_p / \epsilon_o}} \qquad (2.12)$$

where λ_m = wave length and μ_r = relative permeability.

At low frequencies when relative permeability μ_r and ϵ_p / ϵ_o are both high, dimensional resonance may occur in a ferrite of ordinary dimensions.

So summarizing the relaxation effects, we have from equation (2.10) and (2.11) :

	$f \rightarrow 0$	$\rho \rightarrow x\rho_1$
	(low frequency)	$\epsilon \rightarrow \epsilon_1 / x$
when	$f \rightarrow \infty$	$\rho \rightarrow \rho_2$
	(high frequency)	$\epsilon \rightarrow \epsilon_2$

At low frequencies the impedance of the crystallite is negligible as compared to the boundary. At high frequencies the boundary capacitance short circuits the boundary resistance and bulk dielectric properties approach that of the crystallite.

2.3 Microwave Properties of Ferrites:

Ferrites play an important role in microwave technology. The parameters such as anisotropy, Line width, Saturation magnetization, Spin relaxation sine and losses at Gigahertz (GHZ) frequency range determines the applicability of ferrites for such applications. The important microwave parameters are discussed in preceeding sessions.

2.3.1 Ferromagnetic Resonance in Ferrites:

The basic phenomenon of ferromagnetic resonance in ferrites at microwave frequencies was first described by Land and Li (1935) [13]. He based his explanation on gyromagnetic spin resonance taking place in the internal magnetic fields of crystals. Kittle [1948] further suggested that ferromagnetic quantum mechanical in nature, resonance, include the effects of magnetic anisotropy and the dependence of the induced resonance frequency on the shape of the specimen. Resonance is caused by the tendancy of electromagnetic field to align the spins in the material with the instantaneous direction of the magnetic field in the electromagnetic wave. When the energy of the incident field is sufficient, the spins in the material will precess and absorbs energy from the electromagneti wave. This aligning tendancy will be countered by any external field and by anisotropy of the crystal, which binds the magnetization and results in a high resonance frequency [4]. This ferromagnetic resonance occurs at a frequency given by:

$$(w/r)^2 = [\, H_a (1-2\sin^2\theta) + H_{ext} \cos(\theta_o-\theta)\,]\, H_{ext}$$

$$(\sin\theta_o / \sin\theta) \quad (2.13)$$

and $\sin\theta\cos\theta / \sin(\theta_o-\theta) = H_{ext} / H_a$

where w = resonance frequency

Alignment by an external magnetic field permits precession of the spins in only one direction resulting in a non-reciprocal property. For an instance, a wave in one direction can be attenuated as a result of resonance absorption whereas the wave in the opposite direction will propagate with only a normal reflection. This principle has become the basis of useful microwave ferrite systems. The propogation constants are also different for the forward and reverse direction. This behaviour is extremely useful in microwave devices to attenuate undesired (reflected) waves and to shift the phase of a transmitted wave relative to a reflected wave. Based on the principle, the gyrators, circulators and faraday rotation devices are employed.

2.32 Line Width :

It determines sensitivity or sharpness of the resonance in ferrites. This is of considerable importance both shown on theoretical viewpoint and also from application view point. It is a measure of the rate at which energy is transferred from the system of precessing spin dipoles to the lattice vibrations. A rapid transfer results in damping of the precessional magnetization vector, which yields a broad spectral line [15].

The line width arises from two major sources : (i) spin-lattice interaction : It is due to transfer of energy (direct coupling) from uniform precession (all spins in phase) of the spins to lattice at a given thermal equalibrium between spin and lattice. However, this contribution to the ferrite line width is relatively

small. The relaxation time for this spin-lattice process is approximately 10^{-7} second. (ii) Spin-spin interaction: In this case energy is coupled to the lattice by spin-spin relaxation of spin waves inside the ferrite. A spin wave is a nonuniform mode of magnetization precession in which the spins are out of phase. The relaxation time for this spin-spin processes 10^{-9} sec. to 10^{-10} sec.

--

REFERENCES :

1. B.D. Culity, "Introduction to Magnetic Materials", Wesley Publishing Co. 1972.

2. "Magnetic Properties of Metals and Alloys", American Society of Metals, Cleveland (1959).

3. F. Kools, "Factors governing the coercivity of Sintered anisotropy M.type ferrite", Journal De Physique, C6-(1985).

4. J. Smith and H.P.J. Wijin, "Ferrites", Philips Technical Library, Eindhoven (1959).

5. F.G. Brakman, " Magnetic Ceramics" - A review and Status report, American Ceramic Society Bulletin 47, no. 1 186-94, Feb. (1968).

6. D. Hadfield, "Permanent Magnets and Magnetism," London ILIFFE Books Ltd (1962).

7. R.M. Bozoroth "Ferromagnetism", (1951).

8. G.W. Ratheman, "Curie temperature study of M type Hexaferrites" Proc. 3rd Euro Conf. on Hard Magnets. Mat., Amsterdom 7-16 (1974).

9. E.C. Snelling, Soft ferrites, London ILIFFE BOOKS LTD.

10. J.C. Hostetter H.S. Roberts, "Note on the Dissociation of Ferric Oxide in Glass and its relation to colour of Iron Bearing Glasses", Journal of American Ceramic Society Vol. (4), p. 127 (1921).

11. C.G. Koops," Dispersion of Resistivity and Dielectric Constant of some Semiconductors at Audio Frequency", Phy. Rev. Vol. 83, p. 121, (1951).

12. F.G. Brockman, P.H. Dowling and W.G. Steneck," Anomalous behaviour of Dielectric Constant of a Ferromagnetic Ferrite at a magnetic Curie point" Physics Rev. 75, 1440 (1949).

13. B. Nicolaas, "Magnetic Resonance in Ferrites, " Proc. of the I.R.E. Vol. 44 (1956).

14. E.P. Wohlfarth "Ferromagnetic Materials" Vol. (3), North-Holland Publishing Company (1982).

15. C.D. Owens "Analysis of Measurements on Magnetic Ferrites Proc. of the I.R.E. Vol. 41 (1953).

CHAPTER - 3

SYNTHESIS, CHARACTERIZATION, RESULTS AND DISCUSSIONS

ABSTRACT

In this chapter, method of synthesizing pure and Bi_2O_3 oped barium hexaferrite is described. The results of experimental bservations using x-ray diffraction, metallographic, electrical nd magnetic measurements are presented and discussed.

.1 Experimental Part :

.1.1. Synthesis of Hard Ferrite :

The conventional methods of synthesizing hard ferrites ave been presented in Chapter -1. The present work deals with he synthesis of pure and Bi_2O_3 doped barium hexaferrite by eramic method as described in the following sections.

.1.1 (a) Principle:

The metal carbonates are reduced to their oxides when ney are heated at higher temperatures and subsequent heating esults in $BaO-6Fe_2O_3$ as final product. The formation of $BaO.6Fe_2O_3$ s taking place after two intermediate steps [1] as shown elow:

Step I $$BaCO_3 + Fe_2O_3 \xrightarrow{T < 750^\circ C} BaO.Fe_2O_3 + CO_2 \quad (3.1)$$

Step II $$BaO.Fe_2O_3 + 5Fe_2O_3 \xrightarrow{T > 850^\circ C} BaO.6Fe_2O_3 \quad (3.2)$$

In the present case, doping with Bi_2O_3 has been accomplished

by adding required amount of $Bi(NO_3)_2\ 5H_2O$ to the stoichiometric mixture of $BaCO_3$ and Fe_2O_3, which can produce 2% (weight %) of Bi_2O_3. Bismuth nitrate breaks into Bi_2O_3 and nitrogen oxide after heating above 250°C.

$$4Bi\ (NO_3)_3.5H_2O \xrightarrow{250°C} 2Bi_2O_3 + 12NO_2 + 20H_2O + 8O_2 \qquad (3.3)$$

3.1.1 (b) Raw Materials:

The raw materials used in the present investigation for synthesis of hexaferrites are given below.

Material	Make	Quality
Fe_2O_3 powder	Thomas Baker and Co Bombay	AR Grade
$BaCO_3$	Thomas Baker and Co. Bombay	AR Grade
$Bi(NO_3)_2\ 5H_2O$	SISCO research laboratories Bombay	AR Grade
Acetone	Ranbaxy Lab. Ltd., Punjab.	AR Grade

3.1.1 (c) Synthesis Steps:

Fe_2O_3 (ferric oxide), $BaCO_3$ powder and $Bi(NO_3)_2\ 5H_2O$ were taken in required amount and mixed well using acetone as wetting media. The mixture was placed in rotating steel lined down (planetary ball mill) with steel balls (2 :1 proportion by weight). After wet milling for 6 hrs, the slurry mixture was placed in a beaker at 100°C for 2 hours for drying. The dried flakes were reground using mortor and pestle. Above powder was pressed into cylindrical specimens in a hydraulic press at about 2 tonnes/sq.i

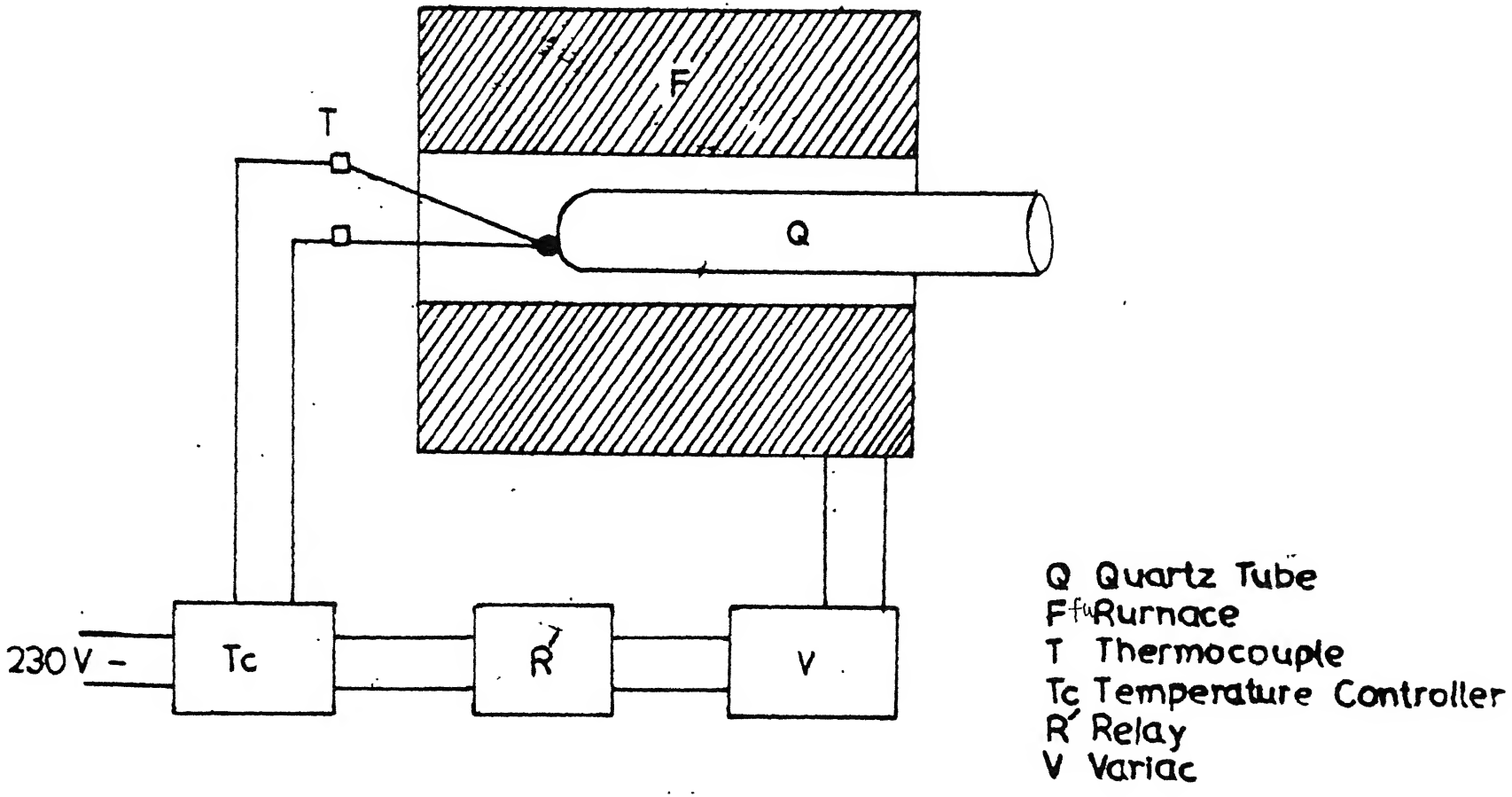

FIG (3·1) Schematic Diagram of Experimental Setup

squinch. Polyvinyl alcohol was used as binder. Then samples were presintered in air at 950°C for 4 hours in a coil furnace. The experimental setup is shown in the Figure (3.1). After presintering and cooling, pellets were again crushed into powder and pressed into pellets using hydraulic press of pressure 4 tonnes/ sq. inch. Final sintering was carried in air at temperatures (1100°C, 1200°C and 1300°C) and for (4,8 and 12 hours). Experimental setup is same as presintering. During sintering the temperature was controlled within ± 1% of the full scale and samples were furnace cooled. The samples were labelled as follows:

Sample specification	Temperature and time								
	1100°C			1200°C			1300°C		
	4 hrs	8 hrs	12 hrs	4 hrs	8 hrs	12 hrs	4 hrs	8 hrs	12 hrs
Pure Barium Ferrite	X1	X2	X3	Y1	Y2	Y3	Z1	Z2	Z3
Bi_2O_3 doped Barium Ferrite	A1	A2	A3	B1	B2	B3	C1	C2	C3

3.2 Characterisation Techniques :

The samples were characterized using electron metallography, X-ray diffraction, mechanical, electrical and magnetic measurements as described below.

3.2.1 X-ray Diffraction Studies:

The X-ray diffraction patterns were recorded with the

help of Siefert Iso-Debylflex diffractometer. For this, samples were crushed into fine powder and mounted on a specimen holder. The CrK filter radiation (λ = 2.291002Å) was used. The diffractometer, goniometer and tube settings fixed at the following values

Tube voltage = 40 kV

Tube current = 35 ma

Counts per second (CPS) = 100

Time constant = 10 mm/ min

Scanning rate = 1.2°/min.

3.2.2 Ultimate compressive strength measurement:

Instron 1195 Instrument was used to determine the compressive strength of the sintered pellets. The load was applied over flat surfaces with head speed of 0.5 mm/min., Chart Speed of 20 mm./min and full scale load of 1000 Kg. to 2000 Kg. were used. The ultimate compressive strength was evaluated from the loads at which samples failed.

3.2.3 Density Measurements:

The sintered density determination was done by liquid immersion method with distilled water as medium. The samples were dried in an oven at 150°C in order to remove the moisture of any trapped gaseous materials. The initial dry weights (W_1) of the samples were taken with an electrical balance. The samples were immersed in a beaker containing distilled water and boiled two hours to allow the water to enter the pores of samples

by replacing the trapped air bubbles. The samples were removed and blotted gently with a tissue paper. The saturated weight (w_2) in air was taken. The samples were then suspended in water and their suspended weight (w_3) was taken. The sintered density was calculated from the following relation:

$$\rho_s = \frac{w_1}{w_2 - w_3} \quad .. \quad .. \quad (3.4)$$

3.2.4 Electrical and Dielectric Measurements:

The sintered pellets (cylindrical) approximately of 1 cm. length and 0.9 cm diameter were given a thin uniform conducting coating of silver paint on opposite flat surfaces to establish ohmic contacts. The resistance (R), capacitance (c) and dissipation factor (Loss tangent- Tanδ) of these samples were measured in parallel mode in the frequency ranges from about 100 Hz to 13 MHz by an impedance bridge (Model 1608A) supplied by General Radio Company of U.S.A. The electrical and Dielectrical parameters were determined as follows [2]:

3.2.4 (a) A.C. Resistivity:

The a.c. resistivity (ρ) were obtained by using the relation

$$\rho = R \times \frac{A}{l} \quad .. \quad .. \quad (3.5)$$

Where R, A and l represent the resistance, area of cross-section and the length of the samples respectively.

3.2.4 (b) Dielectric Constant and Dielectric Loss:

Measuring capacitance at different frequencies, the complex dielectric constants were determined by the relation :

$$C_p = \epsilon_o \epsilon_p \times \frac{A}{l} \quad .. \quad .. \quad (3.6)$$

where ϵ_p, ϵ_p are parallel capacitance and parallel dielectric constant respectively. Similarly knowing loss tangent (tanδ) or dissipation factor at different frequencies the dielectric loss (ϵ_p'') as a function of frequency was calculated as follows:

$$\tan\delta = \frac{1}{\omega C_p R_p} = \frac{\epsilon_p''}{\epsilon_p'} \quad .. \quad .. \quad (3.7)$$

where $\omega = 2\pi f$

Thus dielectric loss $_p = \epsilon_p' * \tan\delta$ ..(3.8)

3.2.5 Magnetic Measurements:

The magnetic properties such as specific magnetization (σ_s), coercivity (H_c) and Curie temperature (T_c) were investigated using the following techniques:

3.2.5 (a) Specific Magnetization : Coercivity and Curie Temperature Measurement:

Ferrite samples of approximate dimension 2.5 x 2.5 x 2 mm were cut and polished for the above measurements. A parallel field vibrating magnetometer (Model 150A) supplied by the

Princeton Applied Research Corporation, New Jersy was employed for magnetization studies. The properties measured at room temperature were specific magnetization and coercive field. Curie temperature measurement was carried out for the Bi_2O_3 doped Ba ferrite sintered at 1100°C for 4 hrs at fixed magnetic field of 8 KOe. Ni-Cr vs Ni-Al Thermocouple and digital multimeter Model (8050 A) were used to measure the temperature.

3.3 Results and Discussions:

The results obtained in the present studies are discussed below.

3.3.1 Density Measurements:

The results of density measurements on sintered pure and doped barium ferrites are presented in Fig. (3.2(a)). It is observed that sintering density is increasing with sintering time and temperature. It is also observed that for doped samples density is higher than corresponding pure samples even at lower temperatures. This may be attributed by the following reason. The doped Bi_2O_3 melts at low temperature(800°C) and this molten bismuth oxide wets ferrite particles readily and promotes liquid phase sintering thereby greatly reducing the sintering temperature and enhanced the densification at lower temperatures itself [3]. For a given time of sintering $\ln D$ vs $\frac{1}{T(\text{sintering temp.})}$ is plotted as shown in the Fig. (3.2(b)) shows a straight line. From the graph it follows the relation:

$$\frac{dD}{dt} = A \exp^{-Q/RT} \quad .. \quad .. \quad (3.9)$$

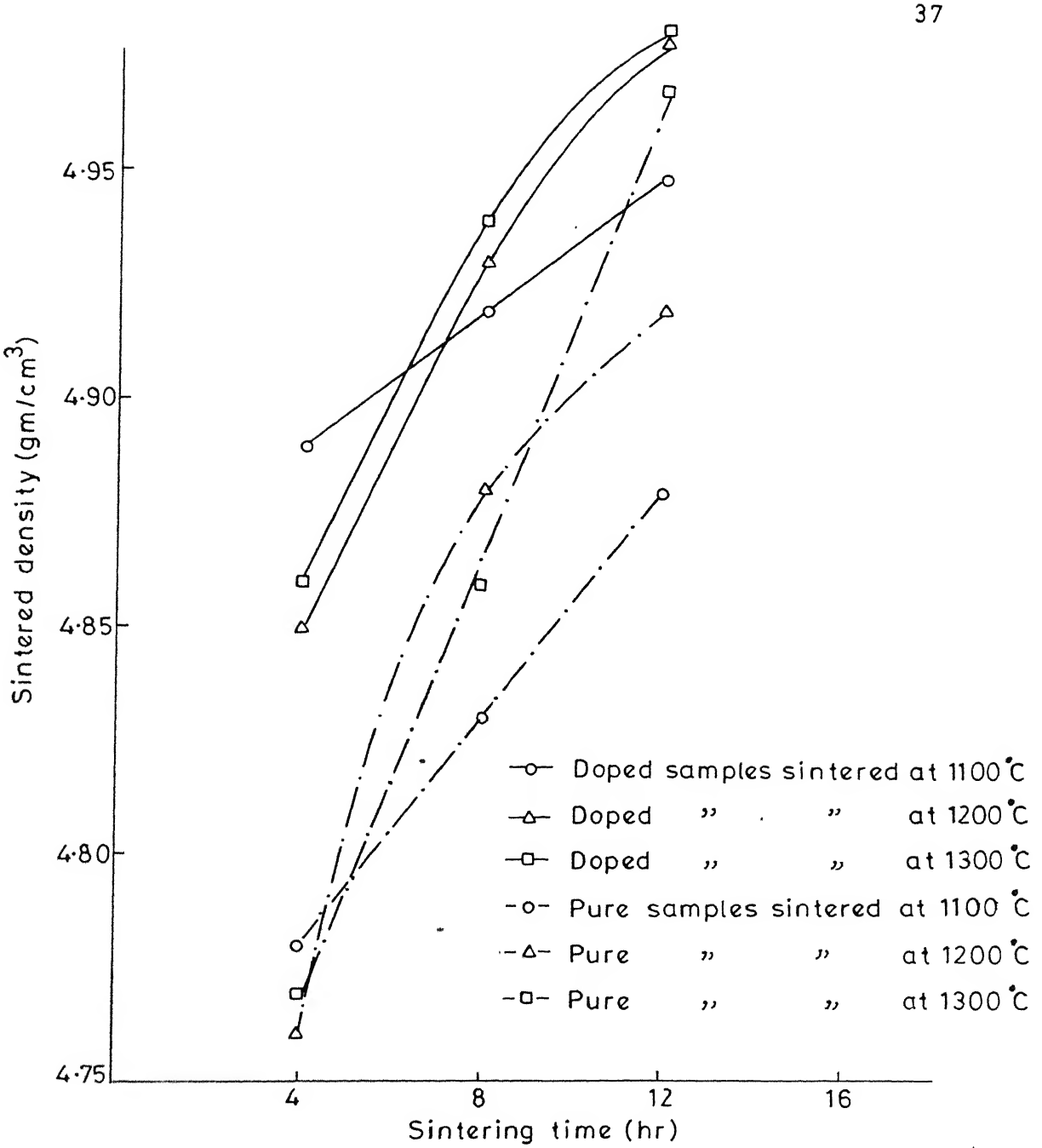

Fig.3·2(a) Variation of sintered density with sintering time

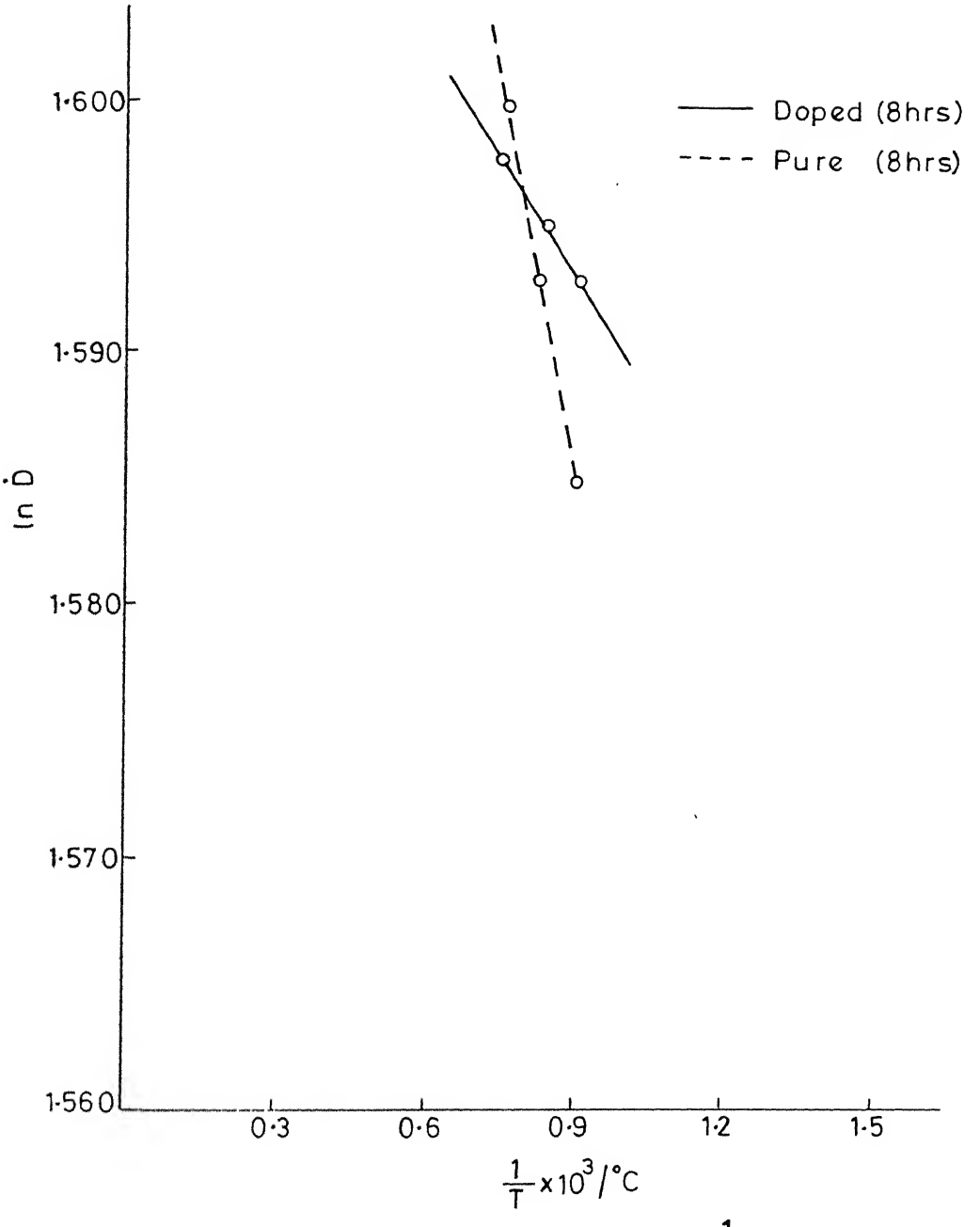

Fig.3·2(b) Variation of ln $\dot{D}$ with $\frac{1}{T}$

3.3.2 Compressive strength:

Results of compressive strength measurement as a function of sintering temperature and time are shown in Fig. (3.3). It is seen that compressive strength is increasing with sintering time and temperature. This might be due to higher sintering densitie at higher temperatures.

3.3.3 X-ray Measurements :

The results of X-ray diffraction studies of pure and doped samples are shown in the Table (3.1) . At lower sintering temperatures it can be seen that λ-Fe_2O_3 phases are also present. At high sintering temperatures intensity of ferrite lines are increasing and it shows the complete ferritization between 1200°C to 1300°C. The observed 2θ, d, I/I_o and (h k l) values for doped and pure samples sintered at 1200°C for 12 hours are shown in the Table (3.2) and also X-ray graphs for these samples are shown in the Fig. (3.4(a) and (b)). The ASTM X-ray diffraction data for barium ferrite, $BaO,Fe_2O_3,BaCO_3$ are given in the table(3.3) (a),(b) (c) and(d) . According to ASTM, the diffraction data for pure barium hexaferrites the most intense lines are 2.62Å (I/I_o = 100), 2.77 Å (I/I_o = 100), 1.625 (I/I_o = 50). However, for doped hexa-ferrites the rdative intensities for these lines are 2.62Å(I/Io=89) and 2.77A° (I/I_o = 100). This may be due to the preferential alignment or due to substitution of bismuth ions for barium in the planes.

3.3.4 Electrical and Dielectric Behaviour:

(a) A.c. Resistivity as Function of Frequency:

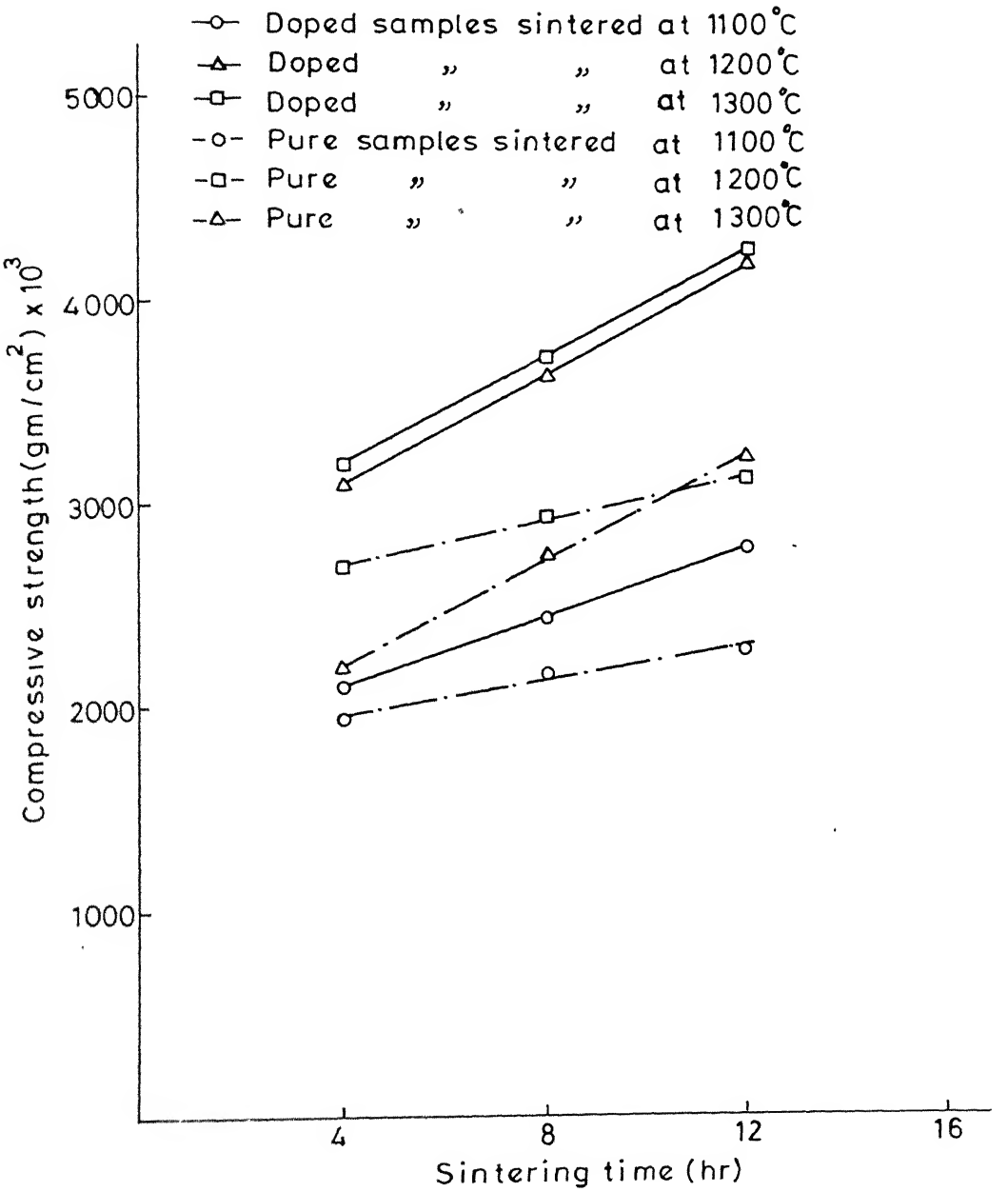

Fig. 3-3 Variation of compressive strength with sintering time

Table 3.1 : Results of X-ray diffraction analysis for various barium ferrite.samples.

Sample Specification	Results of x-ray analysis	Sample Specification	Results of x-ray analysis
A1	$BaO.6Fe_2O_3$, small amount of $-Fe_2O_3$ is also present	X1	Mostly $BaO.6Fe_2O_3$ small amount of Fe_2O_3 is also present.
A2	Only $BaO.6Fe_2O_3$ lines present	X2	Only Ba ferrite lines
A3	Ba ferrite lines	X3	Ba ferrite lines
B1	Ba ferrite lines	Y1	Ba ferrite lines
B2	Ba ferrite lines	Y2	Ba ferrite lines
C1	Ba ferrite lines	Z1	Ba ferrite lines
C2	Ba ferrite lines	Z2	Ba ferrite lines
C3	Ba ferrite lines	Z3	Ba ferrite lines

Table 3.2 : X-ray diffraction data for Bi_2O_3 doped Ba ferrite and pure Ba ferrite samples sintered at 1200°C for 12 hours+

For doped sample (B3)			
2θ (in deg)	d A°	Relative intensity I/I_o	(hkl)
26.56	4.98	2	(101)
28.36	4.67	4	(102)
34.56	3.85	17	(006)
45.84	2.94	45	(110)
46.64	2.89	36	(008)
47.00	2.80	2	(112)
48.76	2.77	100	(107)
51.68	2.62	89	(114)
56.44	2.42	17	(203)
61.66	2.23	22	(205)
65.14	2.12	22	(206)
72.00	1.94	1	(1.0.11)
78.34	1.81	1	(1.1.10)
104.206	1.47	21	(220)

Table 3.2 : Contd.

For pure sample (Y3)			
2θ (in deg)	d A°	Relative intensity I/I_o	(hkl)
26.68	4.96	4	(101)
28.54	4.64	9	(102)
34.60	3.85	11	(006)
45.88	2.93	64	(110)
46.68	2.89	23	(008)
47.44	2.84	6	(11 2)
48.80	2.77	93	(107)
51.88	2.61	100	(114)
56.52	2.41	66	(203)
61.80	2.23	40	(205)
65.24	2.11	25	(206)
72.16	1.94	11	(1.0.10)
78.60	1.80	7	(1.1.10)
102.36	1.47	65	(220)

+All lines are Barium ferrite lines

Table 3.3 (a) : X-ray diffraction data for $BaO.6Fe_2O_3$ (ASTM file no. 7-276)

2θ (in deg.)	d A°	Relative intensity I/I_o	(hkl)
26.81	4.94	10	(101)
28.52	4.65	14	(102)
34.52	3.86	16	(006)
45.86	2.94	40	(110)
46.70	2.89	14	(008)
47.39	2.85	10	(11 2)
48.85	2.77	100	(107)
51.85	2.62	100	(114)
56.50	2.42	40	(203)
61.81	2.23	40	(205)
72.16	1.94	10	(1.0.11)
78.31	1.81	16	(1.1.10)
102.09	1.47	40	(220)

Table 3.3 (b) : X-ray diffraction data for BaO (ASTM file no. 1-0746)

2θ (in deg.)	d A°	Relative intensity I/I_o	(hkl)
41.95	3.20	100	(111)
49.23	2.75	88	(200)
71.95	1.95	75	(220)
87.26	1.66	50	(311)

Table 3.3 (c) : X-ray diffraction data for α-Fe_2O_3 (ASTM file no. 13-534)

2θ (in deg.)	$d_{A°}$	Relati intensity I/I_o	(hkl)
36.47	3.66	25	(012)
50.40	2.69	100	(04)
54.30	2.51	50	(110)
85.34	1.69	60	(116)
101.04	1.48	35	(214)
104.16	1.45	35	(300)

Table 3.3 (d) : X-ray diffraction data for $BaCO_3$ (ASTM file no. 11-697)

2θ (in deg.)	$d_{A°}$	Relative intensity I/I_o	(hkl)
33.11	4.02	65	(111)
38.43	3.48	100	(200)
55.52	2.45	60	(220)
66.15	2.09	30	(311)

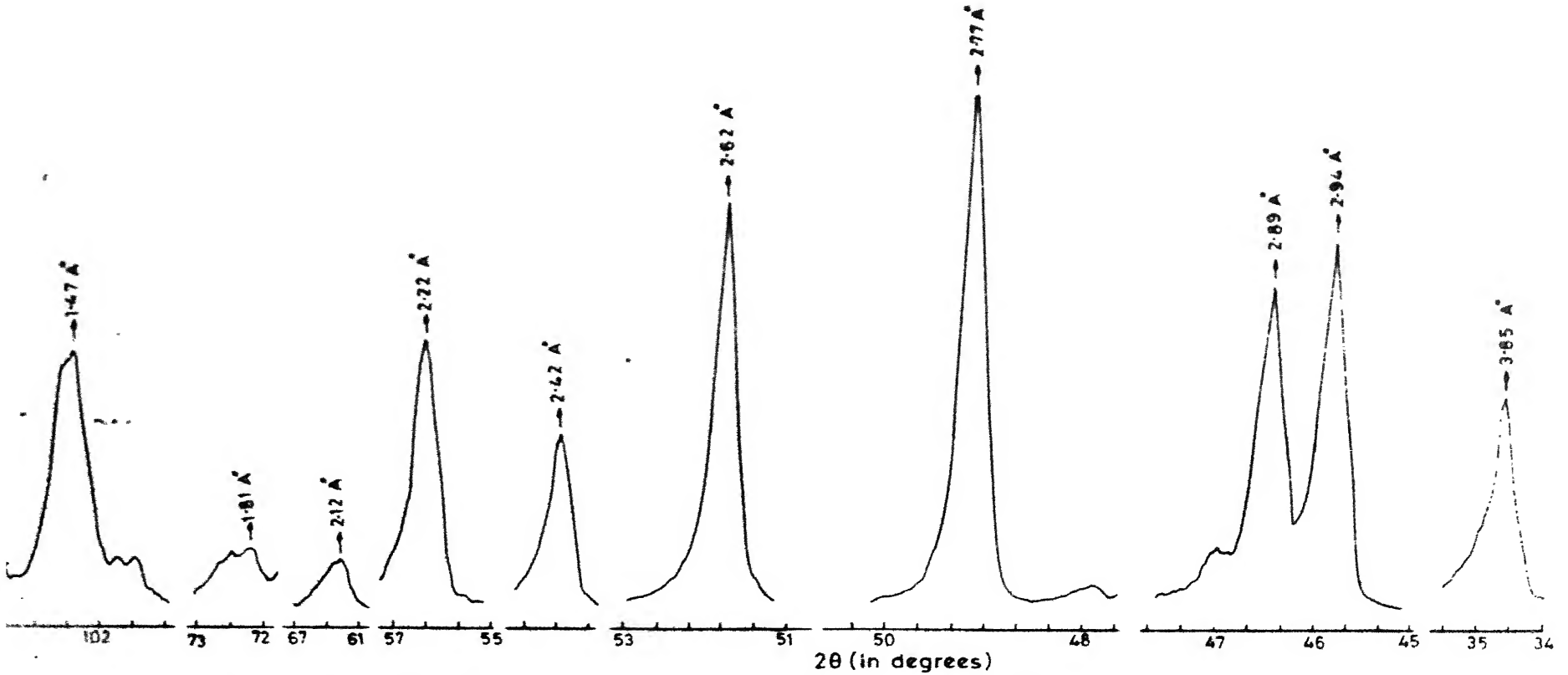

Fig. 3·4(a) X-Ray diffraction pattern of the doped sample sintered at 1200 °C for 12 hrs (B3)

and pure samples sintered at 1100°C, 1200°C for different sintering temperatures are shown in Fig. 3.5(a), (b) (c) and (d). All these samples showed that resistivity decreases rapidly with increasing frequency. This is due to electromagnetic relaxation as a result of structural inhomogeneity. It is also observed that resistivity is increasing with sintering time. However, for the doped samples sintered at 1100°C for 4 hrs. is showing descrepancy i.e. resistivity and decreasing with sintering time. These samples exhibited the presence of Fe_2O_3 unlike others. The frequency dependence of electrical and dielectric parameters of various samples are shown in table (3.4)

(b) Dielectric relaxation :

The variation of dielectric constant ϵ'_p (real part of complex dielectric constant), dielectric loss ϵ''_p, with frequency of the samples sintered at 1200°C for 12 hrs for doped and pure samples are shown in Fig. (3.6 (a) and (b) respectively. These exhibit the following common features:

(i) The dielectric constant (ϵ'), and dielectric losses (ϵ'') are decreasing with the increase of frequency. This may be attributed to the dielectric relaxation as a result of structural inhomogeneity as discussed in section (2.21).

(ii) The doped samples exhibit high value of dielectric constant and losses in comparision to pure samples. This may be attributed to the enhanced local polarization associated with substitution of Bi^{2+} ion in the ferrite lattice.

(iii) Dielectric constant is decreasing with sintering time in both the cases. Dissipation factor given by tanδ is also plotted

Table 3.4 : Frequency dependence of electrical and dielectrical parameters of various barium ferrites samples.

Sample specification	Frequency (Hz)	Resistivity (ρ) Ω-cm	Dielectric constant (ϵ')	Dielectric losses (ϵ'')	Dissipation factor ($\tan\delta$)
A1	100	0.55×10^6	111657.85	385219.58	3.45
	1KHz	0.28×10^6	9531.76	14678.92	1.54
	10KHz	0.06×10^6	2137.43	1774.06	0.83
	100KHz	0.01×10^6	851.05	784.15	2.92
	1MHz	7216.12	263.62	247.80	2.42
	10MHZ	1471.42	73.53	43.01	1.91
	13MHz	1135.50	63.84	33.50	0.52
A2	100	0.13×10^6	264761.1	531110.79	2.06
	1KHz	0.05×10^6	45607.08	6574.90	1.44
	10KHz	0.01×10^6	9241.43	6746.24	0.73
	100KHz	2391.92	4416.68	2592.59	0.58
	1MHz	983.13	2160.33	2657.20	1.23
	10MHz	517.93	617.97	1106.17	1.79
	13MHz	470.00	513.43	919.05	1.79
A3	100	56830.75	6117.10	12173.03	1.99
	1KHz	25857.00	1346.83	2599.39	1.93
	10KHz	12492.24	197.46	268.55	1.36
	100KHz	2199.56	48.29	28.49	0.59
	1MHz	483.16	26.82	19.58	0.73
	10MHz	261.21	15.54	37.04	0.43
	13MHz	249.84	16.63	46.45	0.34

Contd/-

Sample specification	F_{Hz}	ρ Ω-cm	ϵ'	ϵ''	D.F.
B1	100	43862.19	8765.25	18713.82	2.13
	1KHz	13774.26	1259.30	1220.20	0.96
	10KHz	3385.85	396.28	297.21	0.75
	100KHz	536.35	157.04	73.81	0.47
	1MHz	96.95	99.07	53.20	0.53
	10MHz	54.24	199.61	1203.65	6.03
	13MHz	53.01	595.36	7168.37	12.00
B2	100	182872.30	1650.86	2806.47	0.58
	1KHz	41703.19	291.31	191.60	1.48
	10KHz	4447.12	132.63	42.44	3.04
	100KHz	384.03	93.43	18.88	4.75
	1MHz	85.36	80.00	30.40	2.63
	10MHz	51.45	52.41	25.12	1.92
	13MHz	52.78	9.43	3.39	2.77
B3	100	153056.11	1436.73	1724.07	0.83
	1KHz	16502.23	451.31	185.03	2.43
	10KHz	1959.11	298.71	97.08	3.07
	100KHz	528.73	175.53	92.04	0.52
	1MHz	129.12	107.14	81.43	0.76
	10MHz	63.58	8.10	2.26	0.28
	13MHz	64.94	4.39	0.87	0.20

Contd/-

Sample spacification	F Hz	ρ Ω-cm	ϵ'	ϵ''	D.F.
C1	100	87648.75	4675.49	1019.86	2.25
C	1KHz	9367.31	794.20	252.29	0.36
	10KHz	1198.96	528.16	184.85	0.35
	100KHz	378.70	282.65	167.54	0.59
	1MHz	82.92	162.84	122.13	0.75
	10MHz	34.25	9.24	2.03	0.17
	13MHz	34.02	5.00	0.55	0.11
C2	100	98123.89	2044.22	2269.00	1.11
	1KHz	7809.02	794.20	274.00	0.34
	10KHz	2305.91	496.13	312.56	0.63
	100KHz	462.00	192.88	94.51	0.49
	1MHz	74.32	129.03	68.38	0.53
	10 MHz	1.55	14.42	4.09	0.28
	13 MHz	1.56	11.00	4.01	0.19
C3	100	99521.50	1182.00	1825.00	0.88
	1KHz	12121.25	972.50	1010.11	0.75
	10KHz	2100.60	475.22	743.21	0.62
	100KHz	828.48	218.48	646.65	0.79
	1MHz	102.11	172.12	225.08	0.65
	10MHz	55.21	65.80	162.16	0.61
	13MHz	43.41	51.95	88.23	0.59

contd...

specification	F_{Hz}	$\rho_{\Omega cm}$	'	''	tanδ
X1	20KHz	206262.75	77.91	13.94	0.17
	100KHz	21569.96	69.03	12.00	0.08
	1MHz	903.24	64.84	31.25	0.03
	13MHz	275.01	89.64	5.61	0.17
X2	5KHz	1088974.40	1.53	0.72	0.47
	10KHz	439699.10	1.26	0.37	0.30
	100KHz	19313.88	0.98	0.10	0.10
	1MHz	1212.25	0.89	0.61	0.68
	10MHz	10.88	0.53	0.01	0.1
	13MHz	19.51	1.00	0.01	0.01
X3	11KHz	309797.38	0.99	0.17	0.18
	100KHz	13404.69	0.79	0.04	0.05
	1MHz	580.87	0.74	0.01	0.02
	10MHz	373.84	0.84	0.12	0.15
	13MHz	153.40	1.05	0.11	0.11
Y1	12KHz	89496.84	0.94	0.04	0.05
	100KHz	39483.89	0.89	0.02	0.02
	1MHz	250.06	0.79	0.01	0.01
	10MHz	381.67	0.82	0.21	0.26
	13MHz	167.41	1.05	0.13	0.12
Y2	10KHz	352144.19	1.10	0.25	0.23
	100KHz	14955.93	0.91	0.07	0.07
	1MHz	679.81	0.85	0.02	0.03
	10MHz	391.57	0.86	0.16	0.18
	13MHz	129.57	1.09	0.11	0.10

Sample spacification	F Hz	ρ Ωcm	'	''	tanδ
Y3	11KHz	128532.21	1.20	0.31	0.35
	100KHz	89756.00	0.98	0.12	0.21
	1MHz	50222.00	0.83	0.09	0.12
	10MHz	620.21	0.56	0.12	0.24
	13MHz	118.75	0.91	0.08	0.20
Z1	7KHz	265419.00	2.66	0.77	0.29
	10KHz	89140.36	2.50	0.65	0.26
	100KHz	11675.33	1.88	0.23	0.12
	1MHz	653.81	1.66	0.09	0.06
	10.MHz	100.40	1.62	0.22	0.13
	13MHz	58.45	2.02	0.17	0.08
Z2	7KHz	369298.20	2.99	1.25	0.42
	10KHz	277369.94	2.62	1.07	0.41
	100KHz	22189.50	1.59	0.30	0.19
	1MHz	879.65	1.35	0.09	0.06
	10MHz	116.42	1.37	0.17	0.12
	13MHz	89,55	1.75	0.20	0.11
Z3	15KHz	389212.50	3.01	2.89	0.56
	100KHz	110101.50	2.75	2.75	0.65
	1MHz	20195.00	1.65	2.00	0.71
	10MHz	4321.00	1.01	1.65	0.31
	13MHz	809.00	0.01	0.35	0.25

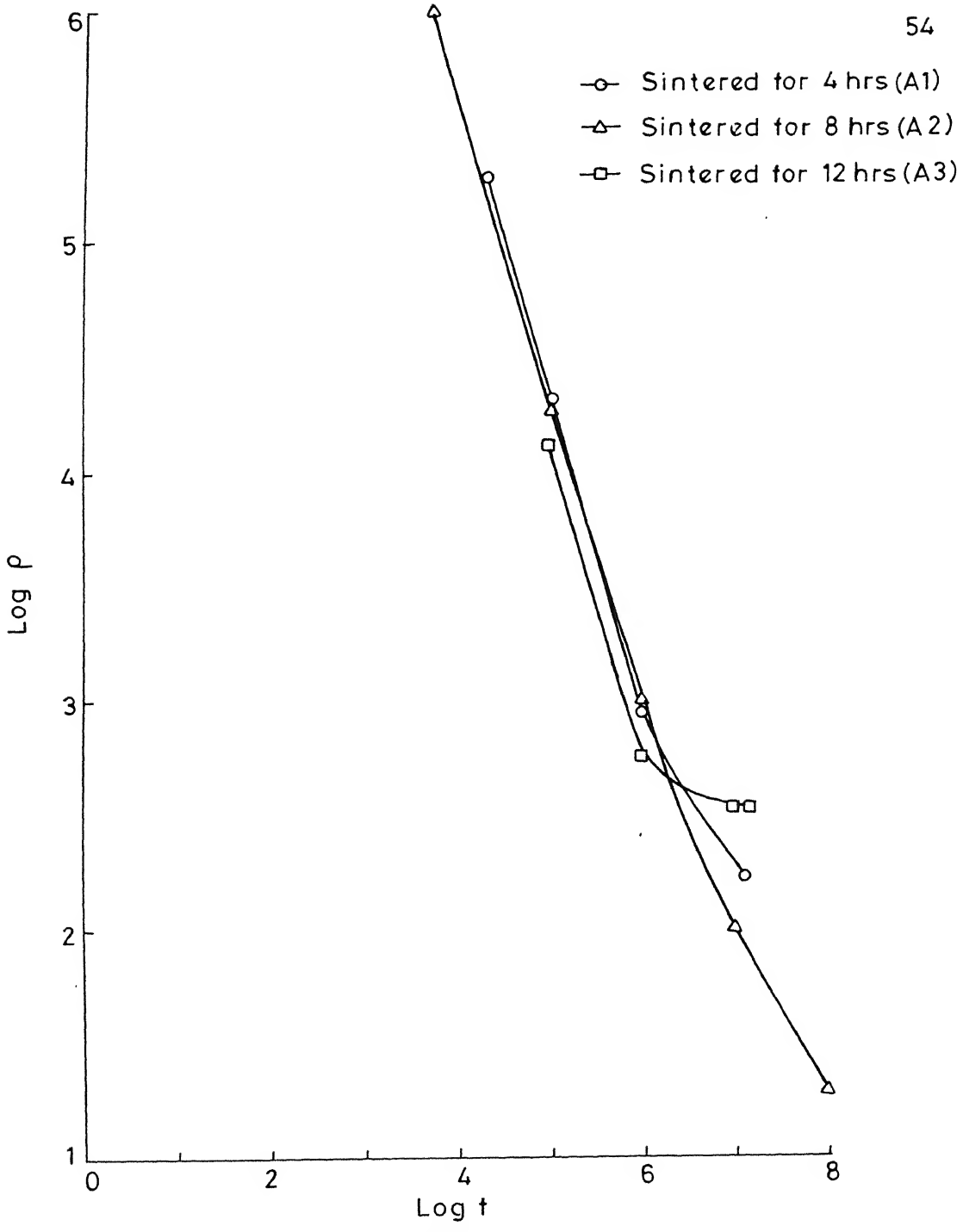

Fig. 3-5(a) Variation of AC resistivity with frequency for the doped samples sintered at 1100°C for 4, 8 and 12 hrs

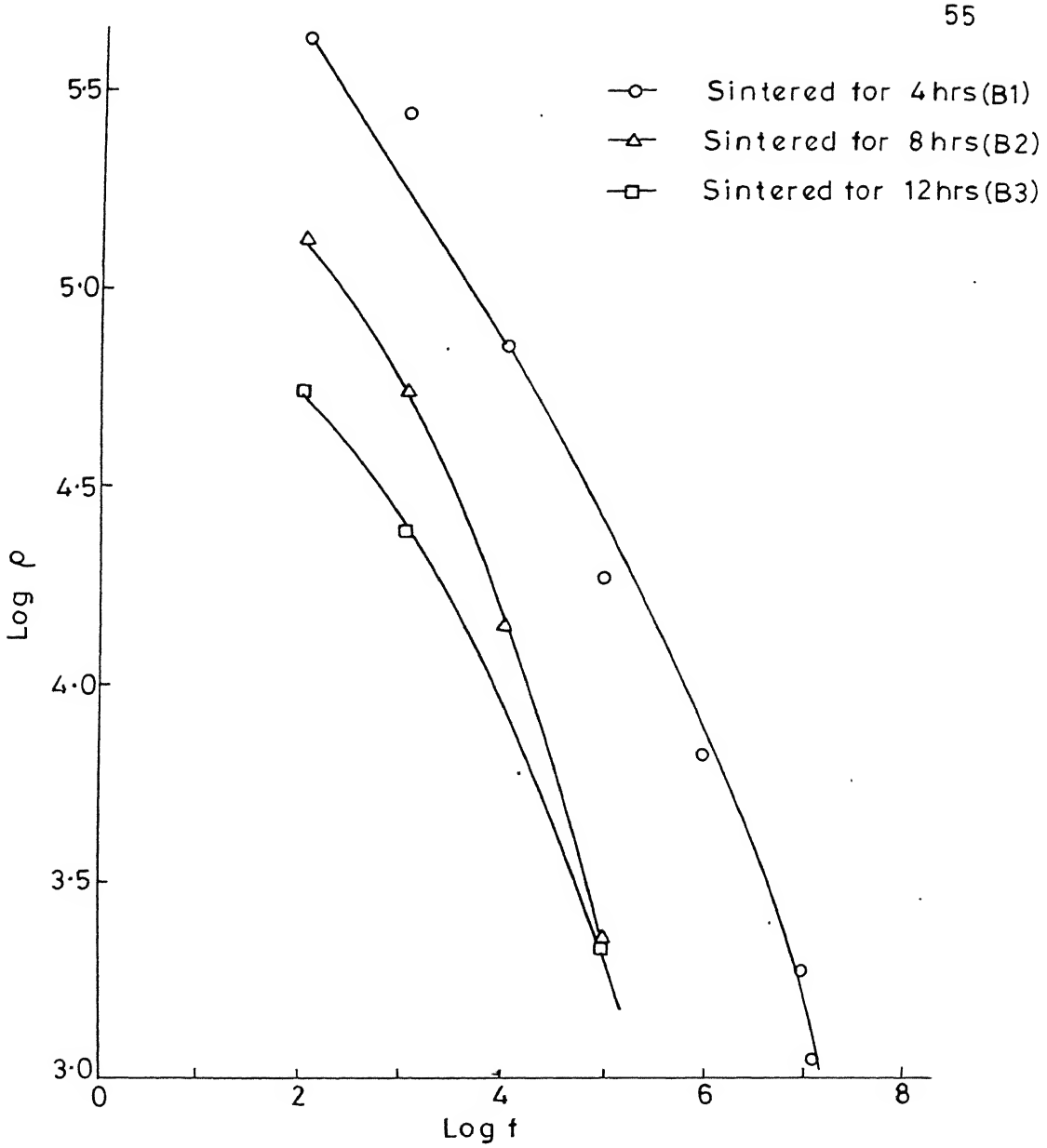

Fig.3·5(b) Variation of AC resistivity with frequency for the doped samples sintered at 1200 °C for 4, 8 and 12 hrs

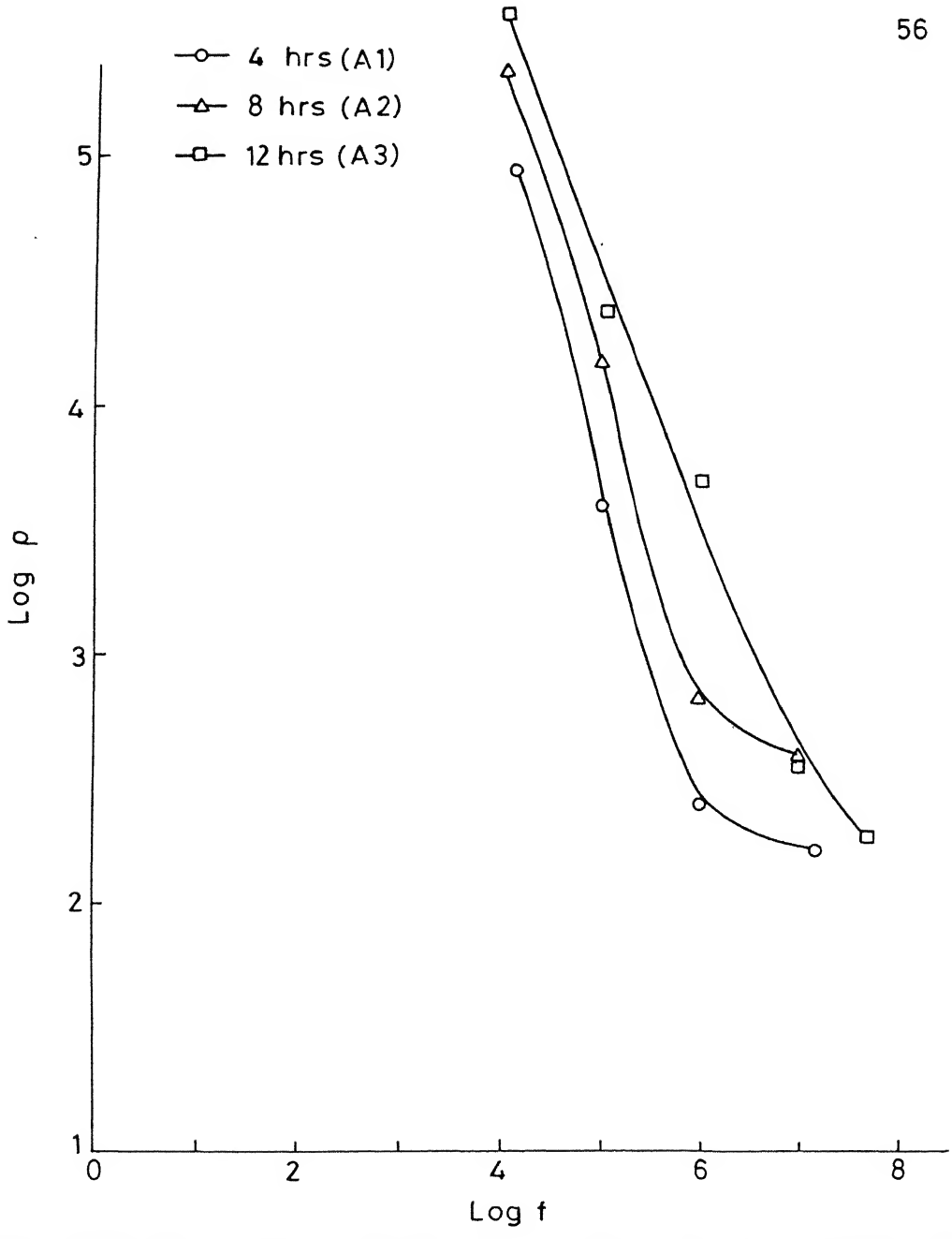

Fig.3·5(c) Variation of AC resistivity with frequency for the pure samples sintered at 1100 °C for 4, 8 and 12hrs

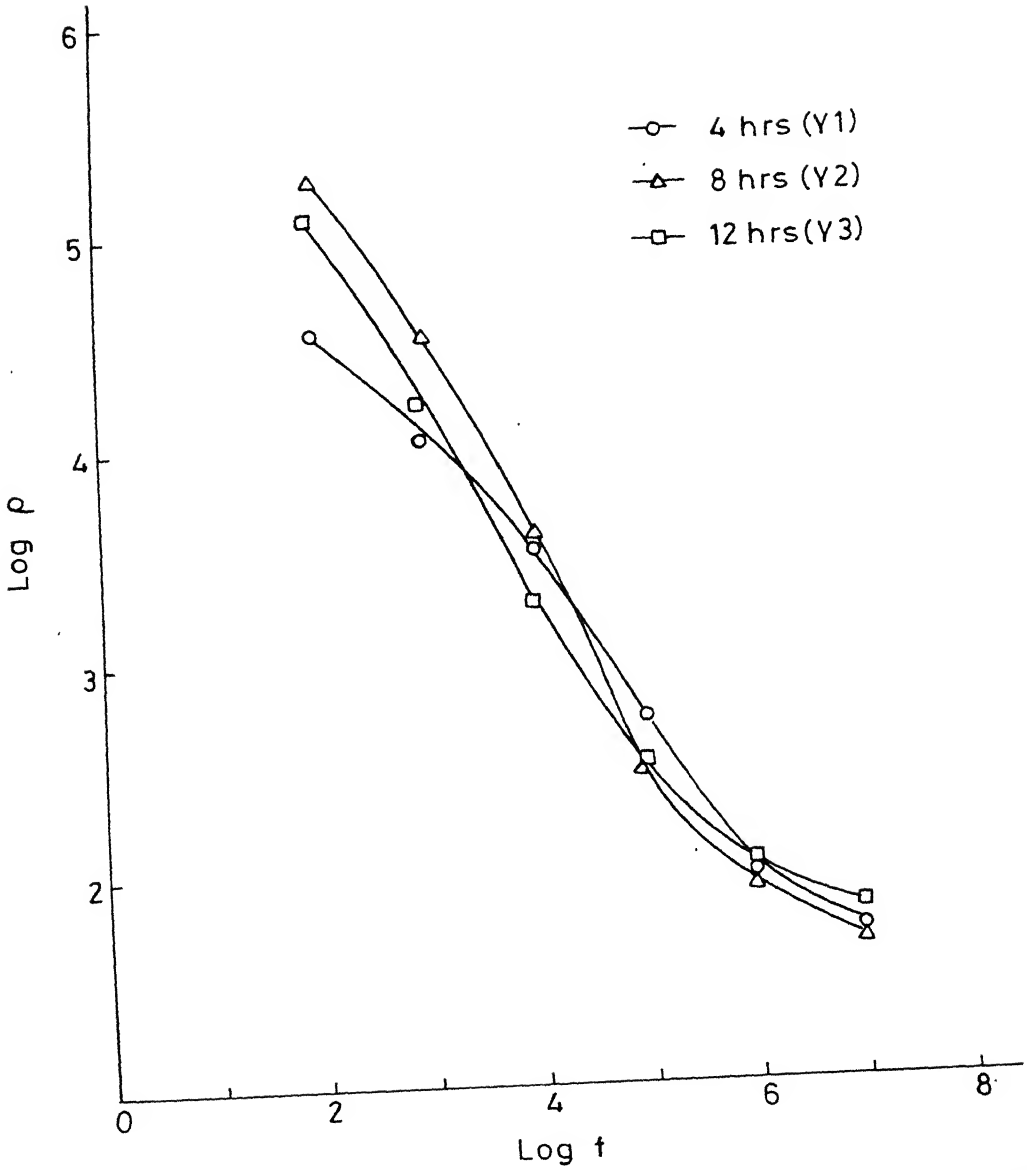

Fig. 3-5 (d) Variation of AC resistivity with frequency for the pure samples sintered at 1200 °C for 4, 8 and 12 hrs

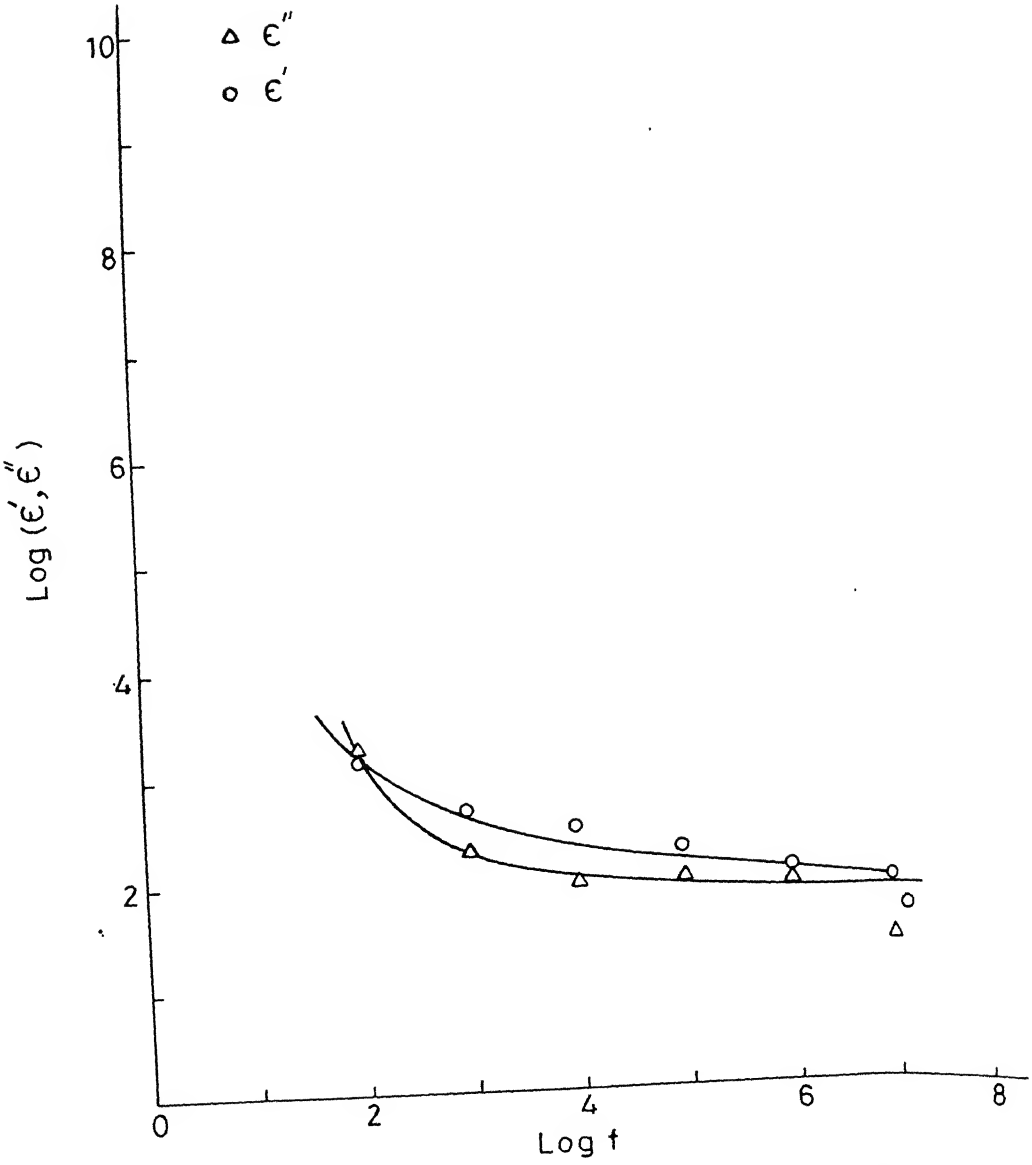

Fig. 3·6(a) Variation of dielectric constant and loss relaxation with the frequency of the field for the doped sample sintered at 1200 °C for 12 hrs (B3)

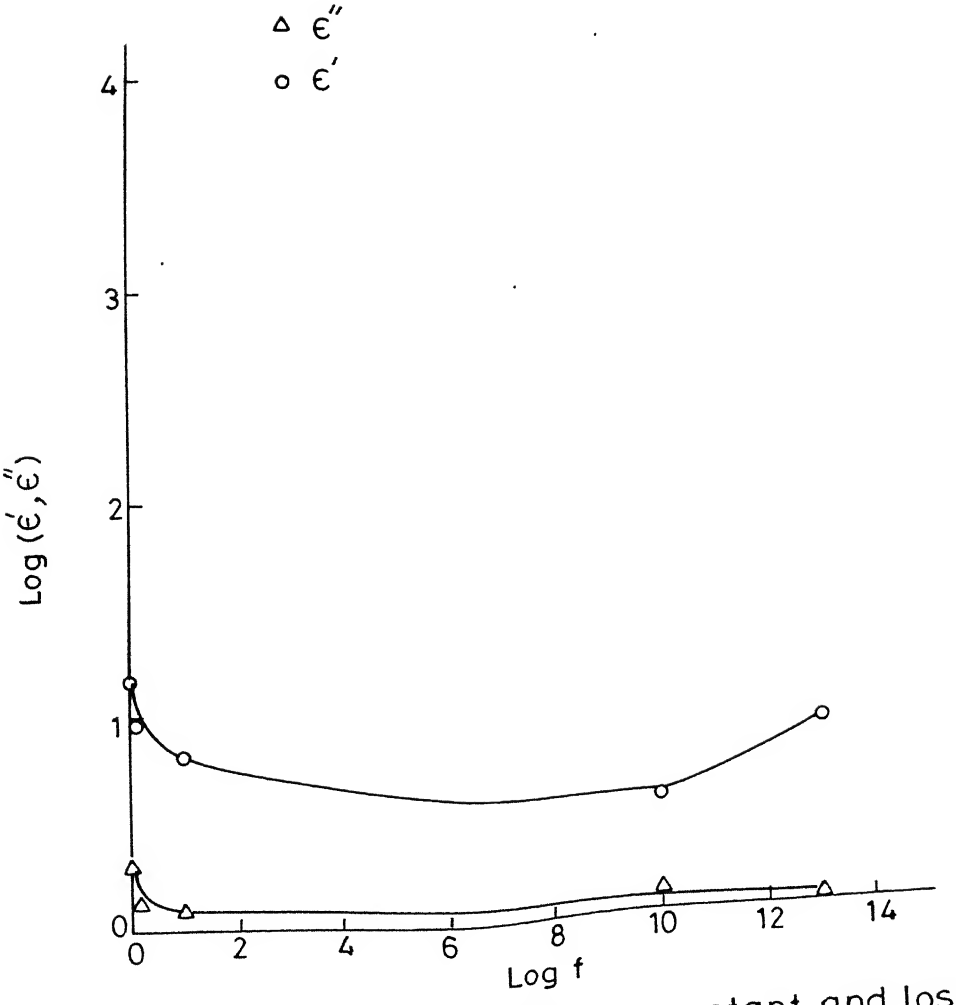

Fig.3·6(b) Variation of dielectric constant and loss relaxation with the frequency of the field for the pure sample sintered at 1200 °C for 12 hrs (Y3)

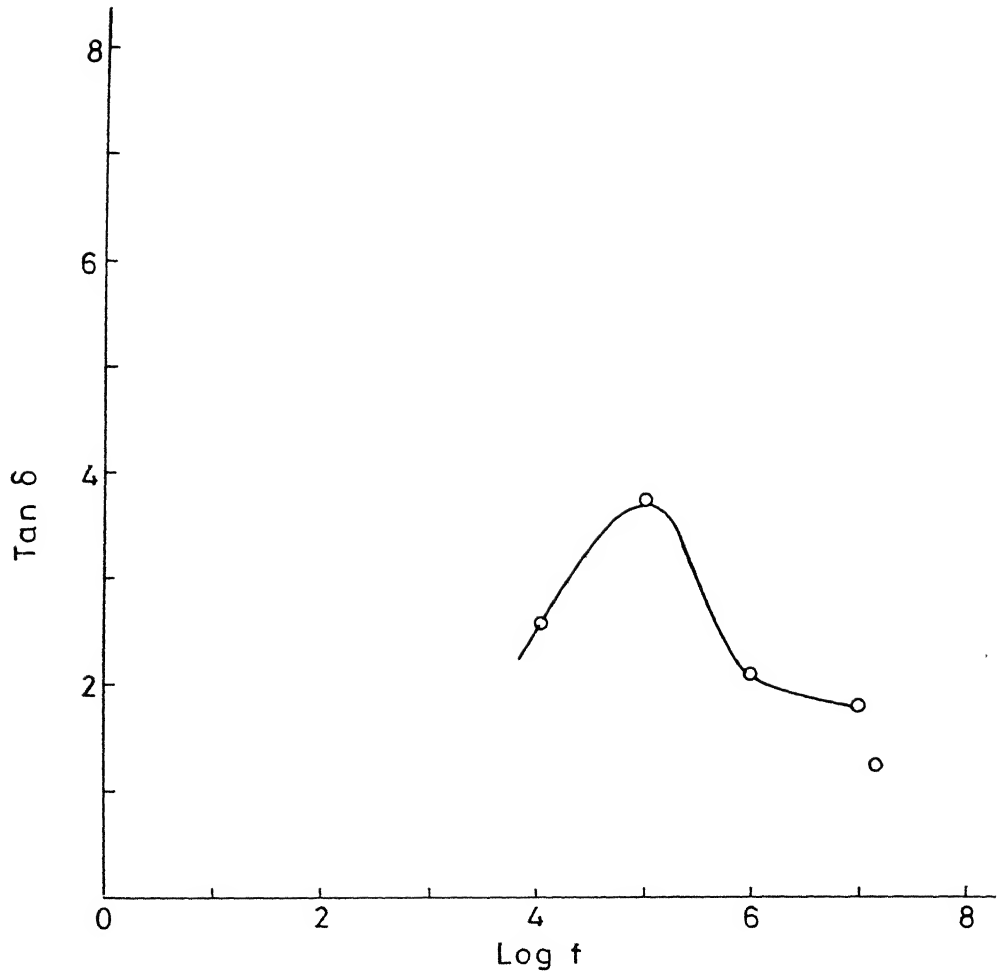

Fig.3·7(a) Variation of dissipation with the frequency of the field for the doped sample sintered at 1200°C for 12 hrs (B3)

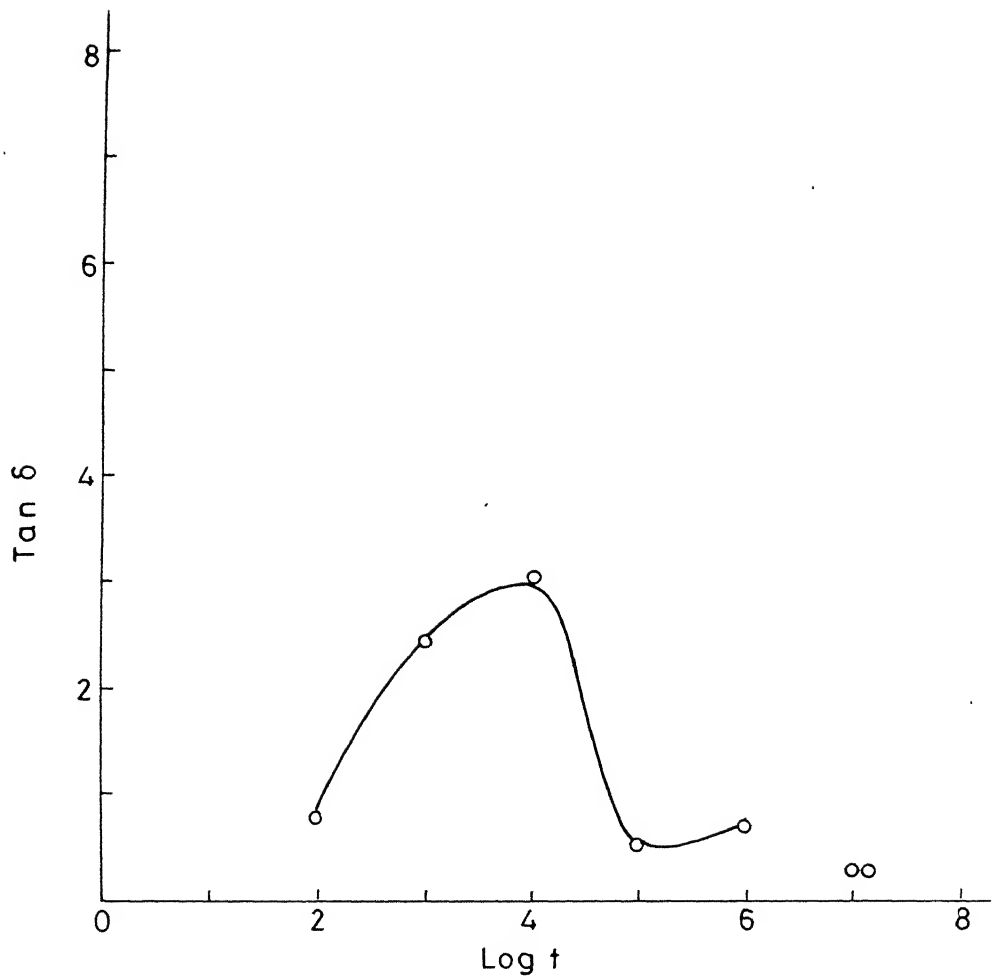

Fig.3·7 (b) Variation of dissipation with the frequency of the field for the pure sample sintered at 1200 °C for 12 hrs (Y3)

with frequency for doped and pure samples sintered at 1200°C/ 12 The plot between tanδ against frequency exhibits cyclic behaviour Such behaviour has been observed by other workers [4]

3.3.5 Magnetic Measurements :

The result of specific saturation magnetization σ_s, remanence Br and coercivity H_c as a function of sintering time and temperature measured at room temperature are summarised in the Table (3.5). The variation of specific magnetisation with field are shown in Fig.(3.8 abc) for pure and doped samples sintered at 1200°C-12 hrs, 1300°C-12 hrs.

From the Table, it can be seen that saturation magnetisatic is increasing with sintering time. However in very few cases 1200°C - 4 hrs(B1), the opposite trend was found. This may be due to inhomogeneity. The coercivity is found to be decreasing with sintering temperature. This may be attributed by the grain growth at higher sintering temperature. For the doped samples lowe coercivity values were found. This may be attributed to the following reason. The effect of Bi_2O_3 on hexaferrites discussed by several workers (5). It seems that Bi_2O_3 changes the unit cell parameter (i.e.) increases 'a' parameter and decreases 'c' parameter (6) thereby it may induce changes in the magneto-crystalline anisotropy in such a way that it decreases coercivity value. The remanent magnetization is decreasing with sintering temperature.

Curie temperature is found for a doped sample 1100°C- 4hrs. which comes out to be 4825°C. Specific magnetization vs temperature graph is shown in Fig. (3.8 e). This is significantly higher than

Table 3.5 : Variation of saturation specific magnetization (σ_s), remanence (Br), coercivity (H_c), and $(BH)_{max}$ with sintering temperature and time.

Sample specification	Saturation specific magnetization (σ_s) emu/gm	Remenant magnetization (Br) emu/gm	Coercive field (H_c) KOe	$(BH)_{max}$ MGOe
A1	56.80	24.03	1.95	0.54
A2	56.97	25.00	2.00	0.59
A3	59.38	26.44	1.30	0.67
B1	59.70	20	1.07	0.37
B2	57.94	20.57	1.06	0.40
B3	56.59	19.90	1.05	0.38
C1	56.71	15.42	0.68	0.22
C2	56.75	18.08	0.86	0.31
C3	57.00	21.93	1.00	0.43
X1	57.80	32.18	3.39	0.93
X2	55.90	32.50	4.17	0.97
X3	56.68	32.38	4.50	0.98
Y1	56.10	33.23	4.59	0.99
Y2	57.50	29.52	4.72	0.81
Y3	57.80	18.00	4.79	0.30
Z1	57.89	21.30	2.49	0.40
Z2	57.92	25.74	2.55	0.61
Z3	57.95	26.65	2.72	0.69

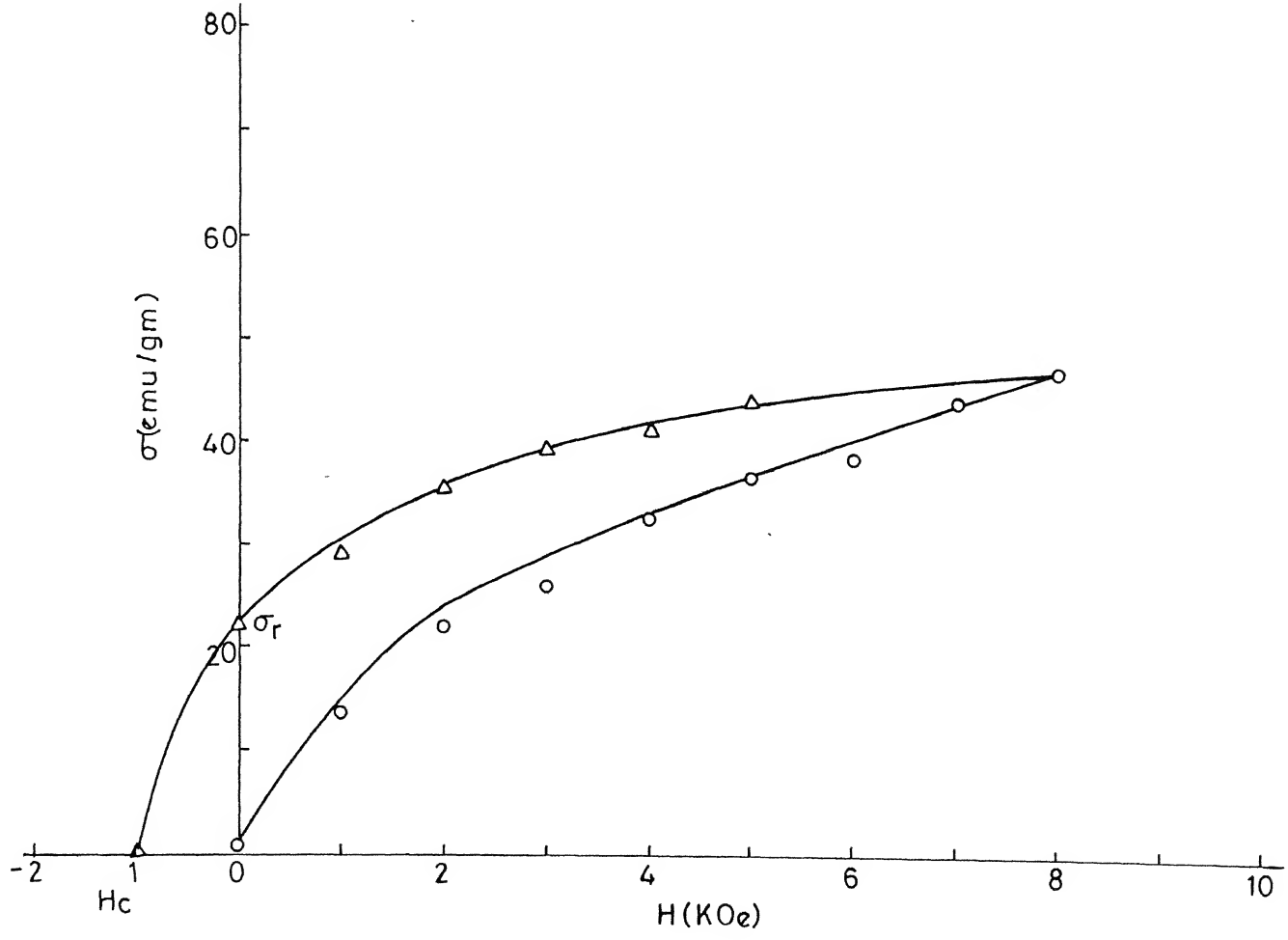

Fig. 3·8(a) Magnetization and demagnetization curve of the doped sample sintered at 1300°C for 12 hrs (C3)

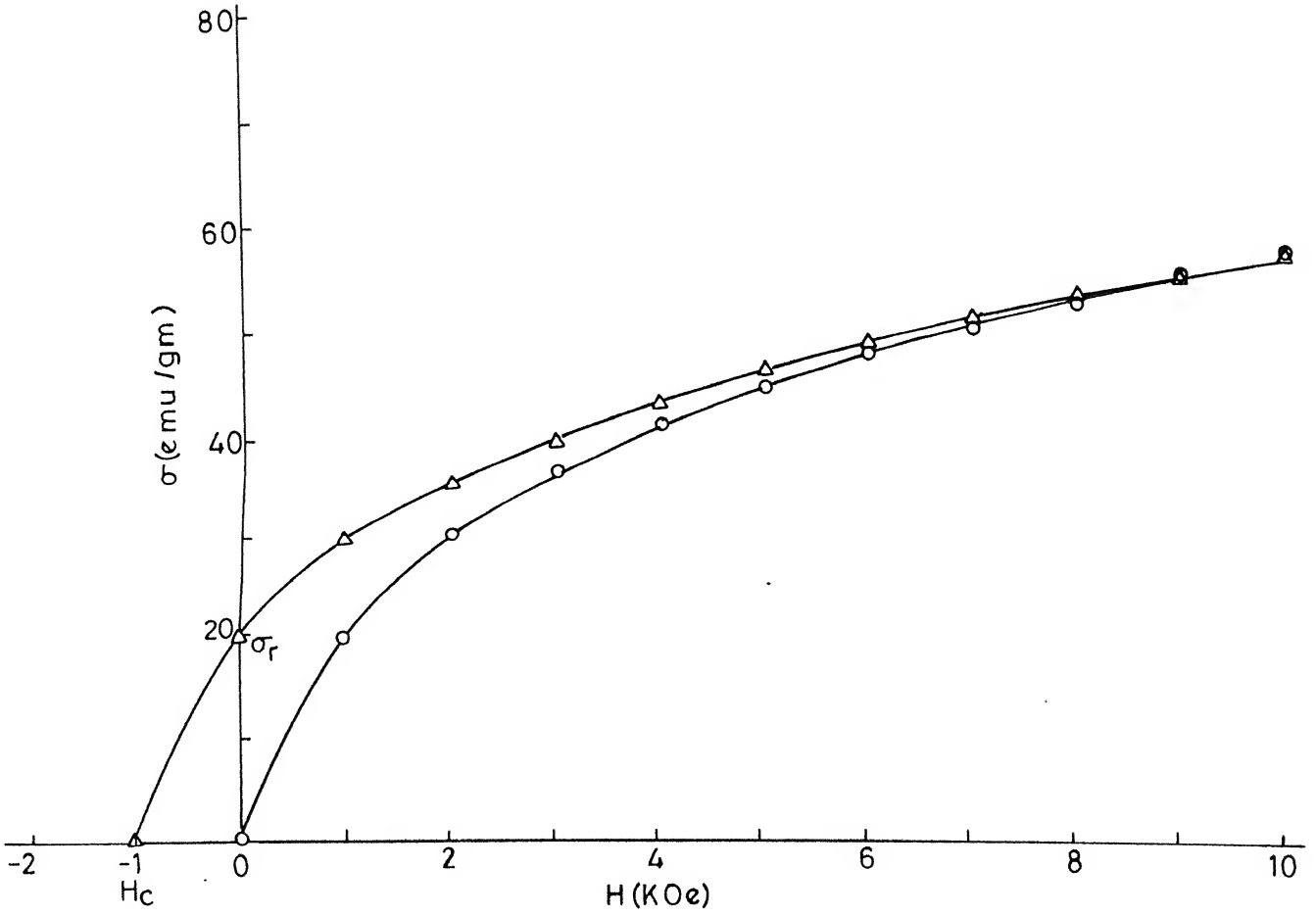

Fig.3·8(b) Magnetization and demagnetization curve of the doped sample sintered at 1200 °C for 12 hrs (B3)

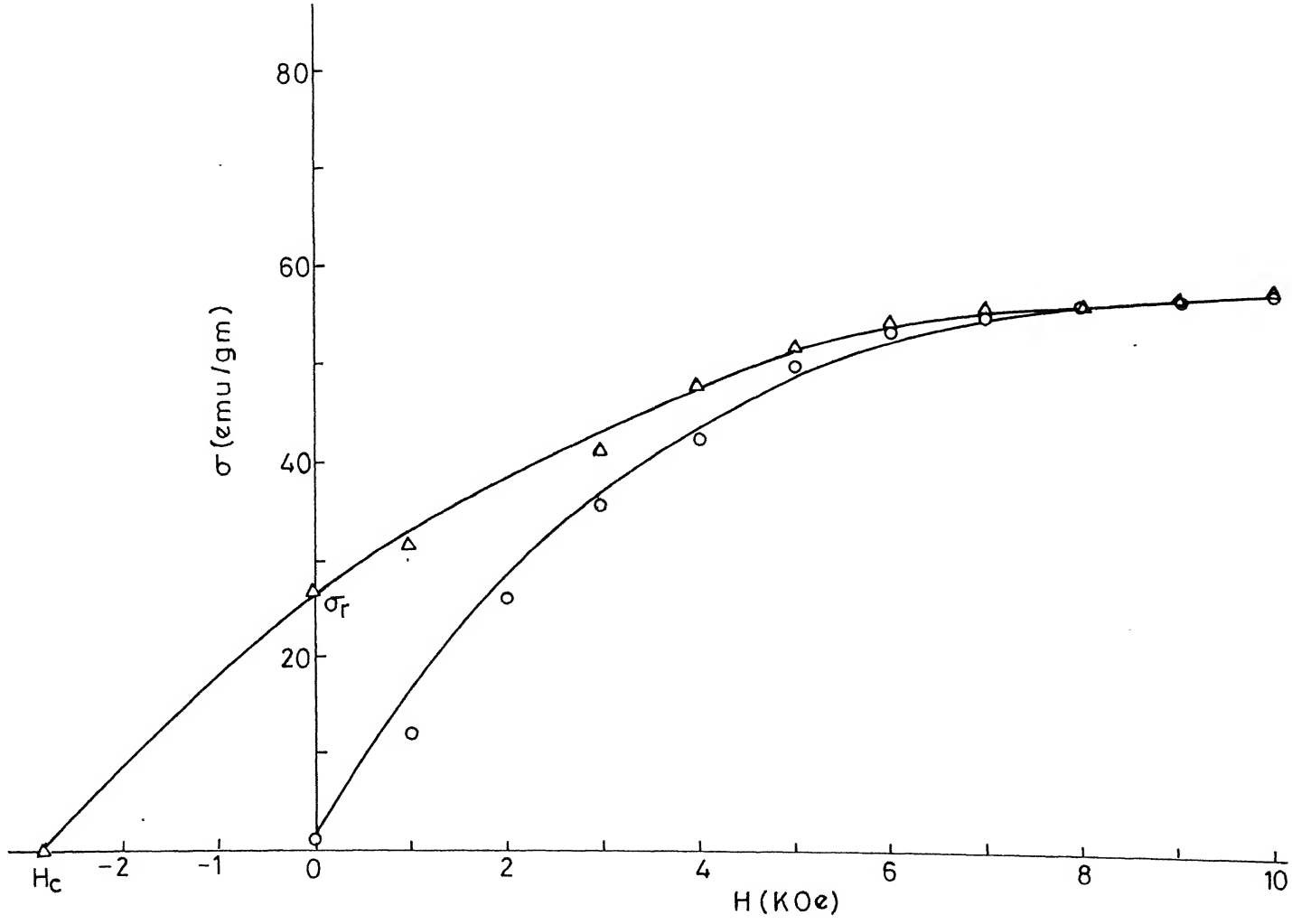

Fig. 3·8 (c) Magnetization and demagnetization curve of the pure sample sintered at 1300 °C for 12 hrs (Z 3)

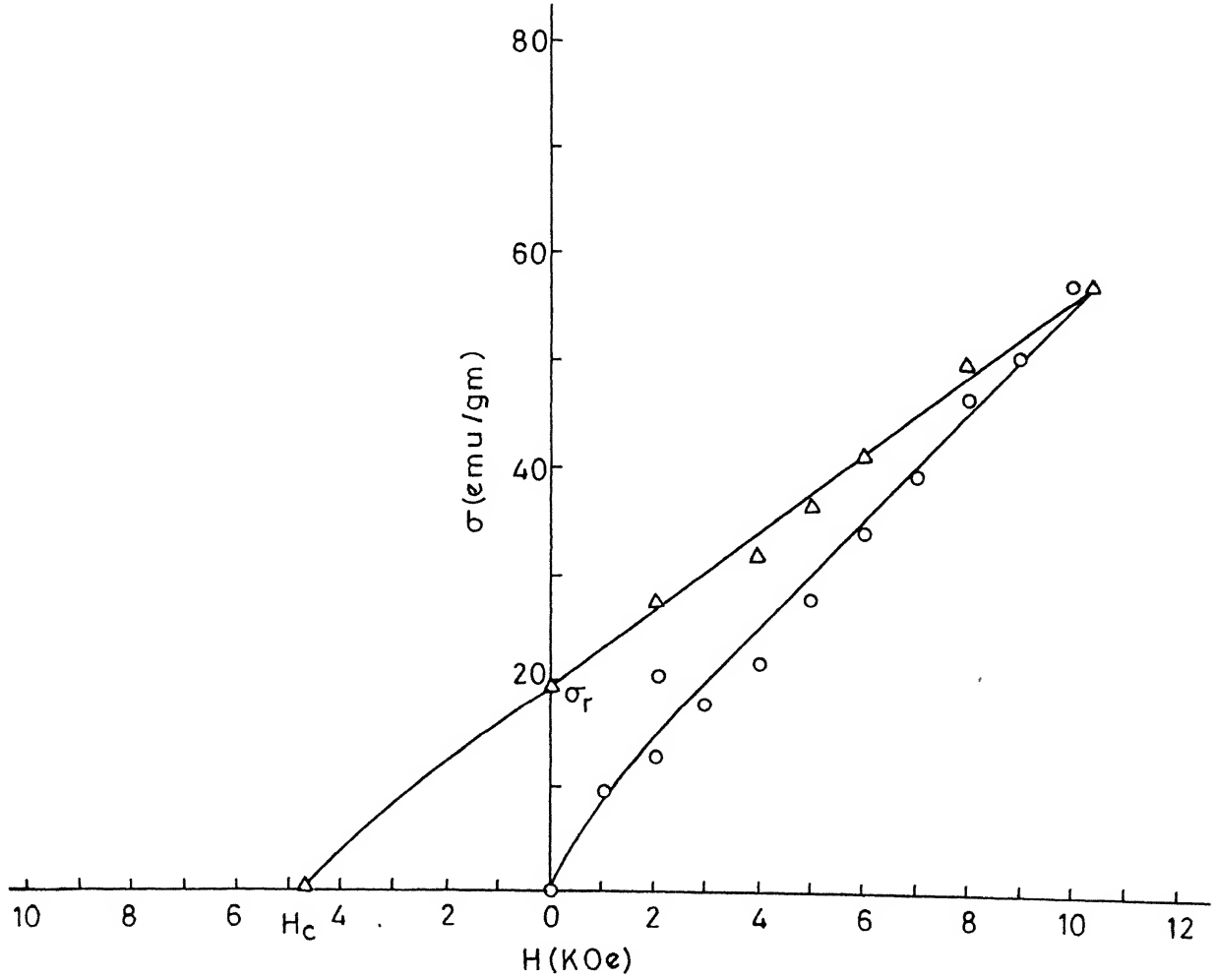

Fig. 3·8(d) Magnetization and demagnetization curve of the pure sample sintered at 1200 °C for 12 hrs (Y 3)

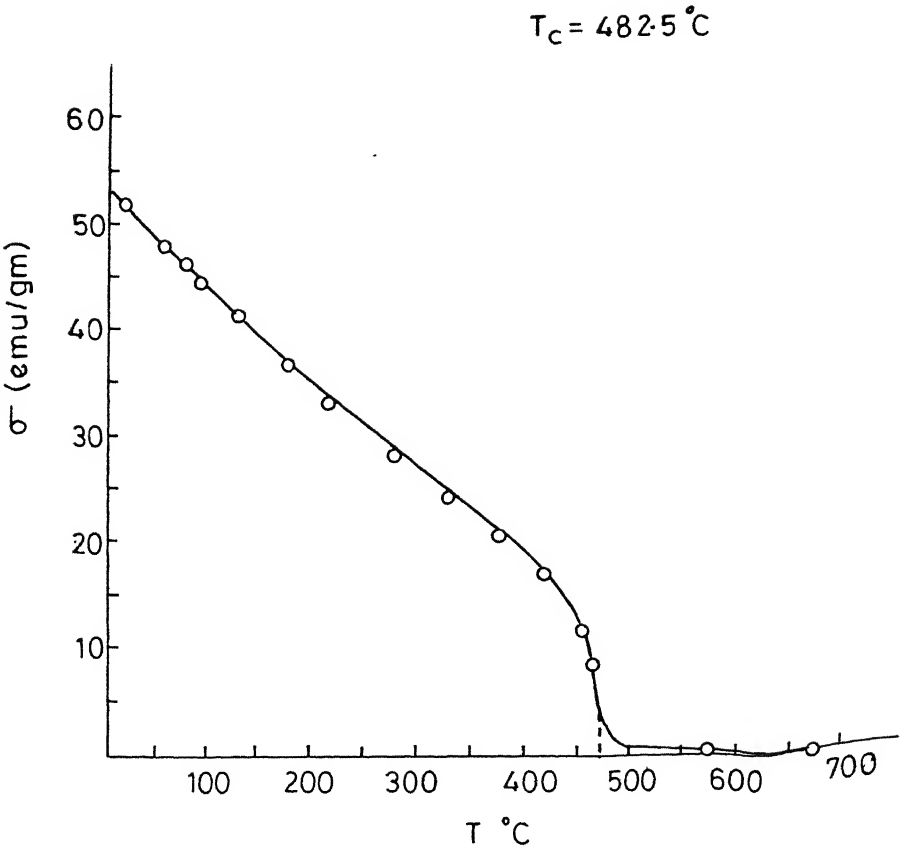

Fig.3·8(e) Saturation magnetization Vs. temperature plot for the doped sample sintered for 4 hrs at 1100 °C (A1)

that of pure sample (T_c = 450°C). This change in T_c may again be attributed to the substitution effect of Bi^{2+} ions for barium sites. Similar effect is known to occur in a Cu doped w-type hexagonal ferrite [7].

REFERENCES :

1. J. Bereketa and M.J. Ridge , " The Reaction between Iron (III) Oxide and $BaCO_3$ in Vacuum, Journal of Chemical Society,p.2463 (1968) .

2. E.C. Snelling, " Properties of Ferrites in Relation to their applications, "Proc. Br. Ceramic Society, 2, 151, (1964) .

3. F.Bradley, " Materials for Magnetic Functions;' Hyden Book Compa Inc. New York.

4. J. Smith and H.P. J. Wijn, " Ferrites", Philips Technical Library, Eindhoven (1959) .

5. P.P. Kirichok, N.B. Voroninia, O.F. Verezhok and V.Ya. Garmash " Effect of Additions of Praseodymium and Bismuth Oxides on the Properties of Barium Hexaferrites', Soviet Powder Metallurgy and Metal Ceramics, Vol. 24, no. 3(267) p. 229 Mar. (1985) .

6. A. Laxi and Benjamin, " Stability of monovalent Cu in the W-type Hexagonal Ferrites", Journal of Magnetism and Magnetic Materials Vol. 61 p. 40, (1986) .

--

CHAPTER - 4

CONCLUSION

The following conclusions may be drawn from the present studies.

1. The complete ferritization occurs in the range of 1 200°C to 1300°C for pure and doped samples.

2. Densification is propotional to sintering time and temperatu In the case of doped ferrites the sintering temperature is lowered as a result of liquid phase sintering.

3. Evidently the ultimate compressive atrength for pure and doped ferrites are found to be propotional to sintering time and temperature. The doped samples invariably exhibit higher compressive strength Fig. (3.3).

4. At low frequencies, the resistivity increases with sintering time. The a.c. resistivity and dielectric constant of these ferrites decrease with increasing frequency. However, tanδ (loss factor) shows approximately cyclic behaviour. At lower frequencies, the doped samples exhibits high resisti-
vi vity in comparision to pure samples. The doped samples exhibits higher dielectric constant and dielectric losses.

5. Magnetic properties obtained for best sample one already given in Fig. (3.8). The doped samples exhibits higher Curie temperature. Coercivity of the pure and doped samples are decreasing with sintering time. It may be due to grain growth at higher temperatures.